Single-cell genomics improves the discovery of risk variants and genes of Atrial Fibrillation

Alan Selewa[1*], Kaixuan Luo[2*], Michael Wasney[3+], Linsin Smith[4+], Xiaotong Sun[2+], Chenwei Tang[5], Heather Eckart[3], Ivan P. Moskowitz[2,6], Anindita Basu[3], Xin He[2#], Sebastian Pott[3#]

[1]Biophysical Sciences Graduate Program,
[2]Department of Human Genetics,
[3]Department of Medicine, Section of Genetic Medicine,
[4]Committee on Genetics, Genomics and Systems Biology,
[5]The College,
[6]Department of Pediatrics,
The University of Chicago, Chicago, IL 60637, USA;
*, +, # These authors contributed equally.

Correspondence: obasu@uchicago.edu, xinhe@uchicago.edu, spott@uchicago.edu

Abstract

Genome-wide association studies (GWAS) have linked hundreds of loci to cardiac diseases. However, in most loci the causal variants and their target genes remain unknown. We developed a combined experimental and analytical approach that integrates single cell epigenomics with GWAS to prioritize risk variants and genes. We profiled accessible chromatin in single cells obtained from human hearts and leveraged the data to study genetics of Atrial Fibrillation (AF), the most common cardiac arrhythmia. Enrichment analysis of AF risk variants using cell-type-resolved open chromatin regions (OCRs) implicated cardiomyocytes as the main mediator of AF risk. We then performed statistical fine-mapping, leveraging the information in OCRs, and identified putative causal variants in 122 AF-associated loci. Taking advantage of the fine-mapping results, our novel statistical procedure for gene discovery prioritized 46 high-confidence risk genes, highlighting transcription factors and signal transduction pathways important for heart development. In summary, our analysis provides a comprehensive map of AF risk variants and genes, and a general framework to integrate single-cell genomics with genetic studies of complex traits.

Introduction

Cardiac diseases are a leading cause of mortality across the world[1,2]. GWAS of cardiac traits have uncovered a large number of associations, including more than 100 loci linked to atrial fibrillation (AF)[3–7]. However, in most loci the disease-driving causal variants remain unknown. Given that

most trait-associated variants are located in non-coding regions[8], researchers often use regulatory and epigenomic datasets to annotate possible effects of variants, and to prioritize putative causal variants[8–10]. Existing datasets, however, were often collected from bulk tissue samples that represent complex mixtures of cell types[11,12], while disease-causing variants often act in specific cell types. Thus, lack of cell type-resolved epigenomic data in disease-related tissues limits our ability of variant annotation and prioritization. Another challenge of post-GWAS analysis is that long-range gene regulation is common, making it difficult to link non-coding variants with their target genes.

Despite these challenges, researchers have made attempts to identify putative risk variants and genes underlying the AF genetics. One study used epigenomic and gene expression data in the human heart to nominate putative risk genes in 104 AF-associated loci. This study, however, did not use rigorous statistical analysis to fine-map causal variants and instead used relatively lenient cutoffs and an *ad hoc* scoring scheme to rank putative target genes[13]. This study nominated nearly 300 genes in these loci, many of which are likely not causal genes. Another study used STARR-seq to map regulatory regions and variants to nominate risk variants in 12 AF-associated loci[14]. But the majority of AF-associated loci were not investigated in the study. A more recent study collected single-cell RNA-seq and ATAC-seq data in the human heart, and performed fine-mapping in AF-associated loci[15]. The study identified 38 putative risk variants in heart CREs. Nevertheless, few nominated variants reach high confidence and in most loci the risk genes remain unknown.

To address these challenges in the context of heart diseases, we developed an integrated framework that unifies advances in single cell epigenomics, computational fine-mapping and a novel procedure for risk gene discovery. Specifically, we performed single-cell chromatin accessibility profiling to map CREs across major cell types in the heart. Our statistical fine-mapping method utilizes the CRE maps to infer disease-relevant cell types and takes advantage of such information to identify putative causal variants. Our novel gene-mapping approach then aggregates information of all fine-mapped SNPs to predict the risk genes, considering multiple sources of information such as distance and chromatin loops between enhancers and promoters. Application of this framework to AF revealed a number of putative risk variants and genes, highlighting biological processes important to the genetics of AF.

68 An unexpected finding from our study is that the majority of risk variants of AF we discovered
69 did not colocalize with heart eQTLs. Taking advantage of our cell-type resolved epigenomic data,
70 we found that this was largely due to the lack of power of bulk eQTL studies to identify regulatory
71 variants with cell-type specific effects. This finding thus sheds light on the common strategy of
72 annotating GWAS results using eQTLs.
73
74 **Results**
75 **Overview of the experimental and computational approach.** Our approach combines single-
76 cell genomics with novel computational procedures to study genetics of cardiac traits (Fig. 1).
77 Using single nucleus RNA-sequencing[16–18] (snRNA-seq) and single cell ATAC-seq (scATAC-
78 seq)[19,20], we obtained transcriptome and open chromatin regions (OCRs) across all major cell types
79 in the adult human heart (Fig. 1, step 1). These OCR profiles allow us to discover cell types
80 enriched with the genetic risks of traits of interest. To identify specific causal variants in trait-
81 associated loci, we performed Bayesian statistical fine-mapping. Fine-mapping is a technique that
82 aims to identify one or few causal variants that explain all the associations in a locus. It avoids the
83 use of arbitrary LD cutoffs in selecting candidate variants and is able to quantify the uncertainty
84 of each nominated variant. Recent fine-mapping techniques are also able to incorporate functional
85 information of variants, such as regulatory activities in trait-related cell types[9,21,22]. Because of
86 these benefits, fine-mapping techniques have been successfully applied to many common traits
87 such as Type 2 Diabetes[23], Schizophrenia[24] and autoimmune disorders[25]. Our fine-mapping
88 method takes advantage of the cell-type-resolved chromatin data to favor variants located in OCRs
89 of enriched cell types (Fig. 1, step 2). After fine-mapping, the candidate SNPs and their associated
90 cell-type information allow us to assign the cell type(s) through which the causal variants are likely
91 to act.
92 Finally, we developed a procedure to infer causal genes at each locus (Fig. 1, step 3), addressing
93 some common challenges. In "gene association tests" researchers test if the set of SNPs near a
94 gene collectively show disease association[26,27]. These types of methods, however, cannot
95 distinguish between multiple genes close to disease-associated variants. Alternatively, researchers
96 may perform fine-mapping first, then link the high-confidence SNPs to target genes using
97 additional information. However, fine-mapping alone rarely leads to a single, or even a few, high
98 confidence SNPs at associated loci [23], therefore this approach also has limited utility. In contrast,

99 our procedure aggregates information of all fine-mapped variants in a locus to nominate risk genes.
100 To see its benefit, suppose fine-mapping in a locus implicates 10 putative causal variants without
101 any single one reaching high confidence; however, if all 10 SNPs likely target the same gene, we
102 can be confident of the causal gene. We developed a statistical procedure to implement this idea,
103 and estimated a score, called gene PIP (Posterior Inclusion Probability), for each gene. Under
104 certain assumptions, we showed that the gene PIP estimates the probability of a gene being causal.
105 The details are described below (Fig. 5a) and in Methods.
106
107 **Single-cell transcriptome and chromatin accessibility profiling reveals multiple cell types in**
108 **the human heart.** We performed snRNA-seq and scATAC-seq using the Chromium platform
109 (10x Genomics) (Fig. 1, step 1). The heart samples were obtained from the left and right ventricles
110 (LV and RV), the interventricular septum, and the apex of three adult male donors (Supplementary
111 Table 1). After quality control, we retained data of 49,359 cells in snRNA-seq and 26,714 cells in
112 scATAC-seq, respectively (Extended Data Fig. 1 and 2).
113 We characterized cell populations with clustering analysis in both snRNA-seq and scATAC-seq
114 datasets. From snRNA-seq[28], we identified eight major cell types based on marker genes and
115 comparison to published single-cell heart atlas data[17] (Fig. 2a, left, Extended Data Fig. 3a), with
116 ~70% of cells from cardiomyocytes (CMs), fibroblasts, and endothelial cells. Clustering based on
117 scATAC-seq data[29] revealed similar cell populations (Fig. 2a, right). We computationally
118 transferred cluster labels from snRNA-seq onto scATAC-seq clusters[28] (Methods) and
119 unambiguously identified matching cell types (Extended Data Fig. 3b, c). Indeed, expression and
120 chromatin accessibility near marker genes showed high cell-type specificity (Fig. 2b, c). Across
121 the eight clusters, gene scores inferred from scATAC-seq, a metric that summarizes the chromatin
122 accessibility near a gene[29] (Methods), were highly correlated with transcript levels in the matched
123 clusters (Extended Data Fig. 3d). We also found good agreement between cell types identified in
124 our scATAC-seq data and a recent study (Hocker *et al.*[15]), the only differences in annotation
125 between these two studies was that we did not detect atrial cardiomyocytes, owing to our use of
126 ventricular samples, and that we detected separate pericytes and smooth muscle clusters (Fig. 2a),
127 whereas Hocker *et al.* annotated a single large cluster as "smooth muscle". These results supported
128 our cell-type assignments in both modalities.
129

130 **Analysis of scATAC-seq data identifies cell-type-specific regulatory elements and their**
131 **regulators.** We pooled cells of the same cell type and identified OCRs separately in each cell type.
132 Combining samples of the same cell type (Extended Data Fig. 4a, b), we detected 45,000-150,000
133 OCRs per cell type (Extended Data Fig. 4c) yielding a union set of 352,904 OCRs. *K*-means
134 clustering of these regions based on their accessibility suggested that most OCRs are active in
135 specific cell types (Fig. 3a). Using differential accessibility (DA) analysis, we identified 173,782
136 (49%) OCRs with cell-type-specific accessibility (Methods). We divided the remaining 179,122
137 (51%) OCRs into three categories based on their detection across cell types: shared in 2-3 cell
138 types, shared in >=4 cell types (denoted as Shared 2-3 and Shared 4), and remaining ones, denoted
139 as "non-DA OCRs", which mostly comprise peaks with low read counts (Methods). In agreement
140 with previous observations, shared OCRs were enriched in promoter regions[30] (Fig. 3b, c).
141 We compared our OCRs to regulatory regions identified in multiple tissues in ENCODE[12]. As
142 expected, a large fraction of OCRs from major heart cell types (e.g., CMs, endothelial, fibroblasts)
143 overlapped with DNase Hypersensitive sites (DHS) from the ventricles (Fig. 3d, top, Extended
144 Data Fig. 6). In contrast, the proportions of OCRs from rare cell types (e.g., myeloid) overlapping
145 with bulk DHS were significantly smaller, suggesting that scATAC-seq is more sensitive and
146 detects more regulatory elements specific to rare cell types compared to bulk DHS (Fig. 3d, top,
147 Extended Data Fig. 5d). This can be seen in several cell-type-specific OCRs near marker genes of
148 rare cell types, which were largely undetected in the pseudo-bulk sample (Extended Data Fig. 4).
149 Additionally, 60-80% of OCRs from major cell types overlapped with H3K27ac regions from LV
150 and RV, suggesting enhancer activities (Fig. 3d, bottom, Extended Data Fig. 6). Together, these
151 results showed that scATAC-seq identified cell-type-specific regulatory elements. We also
152 compared cell-type-specific OCRs identified in our study to peaks identified by an earlier single-
153 cell study in heart[15] and found that OCRs showed good agreement across studies (Extended Data
154 Fig. 7). Importantly, more than 75% of OCRs detected in our CMs were also detected in ventricular
155 CMs by Hocker *et al.* (Extended Data Fig. 7).
156 Chromatin accessibility is largely controlled by lineage-specific transcription factors (TFs)[31].
157 To identify these TFs, we assessed the enrichment of TF motifs in OCRs specific to each cell type
158 and identified 260 significantly enriched motifs (Methods). Because TFs of the same family may
159 share similar motifs, we performed additional analysis to infer the exact TFs driving the
160 enrichment, assuming that for these TFs, their motif enrichment should correlate with gene

161 expression across cells. To test this, we correlated motif accessibility scores of TFs calculated by
162 chromVar[32] with their accessibility-derived gene scores, a proxy for gene expression[29] (Methods).
163 This analysis yielded 76 TFs with enriched motifs and correlation > 0.5 (Fig. 3e, Supplementary
164 Table 2). Many of these TFs are cell type-specific (Fig. 3e) and include known CM regulators,
165 such as TBX5, GATA4, and MEF2A[33] (Fig. 3f). These results provided a compendium of putative
166 transcriptional regulators across major cell types in the human heart.
167
168 **Open chromatin regions in CMs are enriched with risk variants of heart diseases and inform**
169 **statistical fine-mapping.** Using our cell-type-resolved OCRs, we assessed the contributions of
170 different cell types to genetics of heart-related traits[34]. Risk variants of AF were almost exclusively
171 enriched (>10-fold) in OCRs from CMs (Fig. 4a). Similar findings were reported in an earlier
172 study[15]. Interestingly, the variants associated with the PR interval showed a similar enrichment
173 pattern, suggesting a genomic link between PR interval and AF risk for future investigation[35] (Fig.
174 4a). In contrast, risk variants of cardiovascular traits and diseases, and blood pressure, were
175 enriched across multiple cell types (Fig. 4a). As control, non-cardiovascular traits showed little or
176 no enrichment in heart cell types (Fig. 4a). We also checked the enrichment of genetic risk of AF
177 at open chromatin regions at individual cells, using the method SCAVENGE[36]. This analysis
178 confirms that the vast majority of cells enriched with AF risk are CMs (Extended Data Figure 8).
179 Together, these results suggest distinct cell type origins of different heart-related traits,
180 highlighting CMs as the main cell type underlying AF.
181 This observation motivated us to take advantage of the epigenomic data to statistically fine-map
182 causal variants in 122 approximately independent AF-associated loci[37]. We first used TORUS[21] to
183 estimate how putative risk variants are enriched in multiple functional annotations, including
184 protein-coding regions, conserved sequences, and OCRs in CMs (Extended Data Fig. 9a,
185 Methods)[21]. This information was used to set prior probabilities of variants being causal. We then
186 performed fine-mapping analysis of all AF-associated loci with SuSiE[38]. Compared to fine-
187 mapping that treats all variants equally (uniform prior), this procedure increased the number of
188 high-confidence risk variants. In total, we identified 68 variants whose probabilities of being causal
189 variants, denoted as Posterior Inclusion Probabilities (PIP), are 0.5 or higher, compared with 44 at
190 PIP >= 0.5 under the uniform prior (Fig. 4bc, Supplementary Table 3, Extended Data Fig. 9bc).

191 Across 122 loci, our procedure narrowed down putative causal variants to 5 or fewer SNPs in 51
192 loci (Fig. 4d).
193 We highlighted the advantage of our functionally informed fine-mapping with some examples.
194 In the locus containing HCN4, several SNPs are in high LD with similar GWAS association
195 statistics (Fig. 4e, top). Our procedure identified a single SNP, rs7172038, as the most likely causal
196 variant (PIP = 0.99) in the locus (Fig. 4e, middle). This SNP is inside a CM-specific OCR, and
197 H3K27ac region in the heart. Interestingly, the Activity-by-contact (ABC) method [39] predicted a
198 loop between the SNP and the HCN4 gene. HCN4 is an ion channel and has been implicated in
199 the genetics of AF[14]. In another example, we nominated a likely causal variant (PIP = 0.96) among
200 several high LD variants in the locus containing GATA4 (Extended Data Fig. 9d), an important
201 TF for AF[40].
202 A recent study nominated putative causal variants in 12 AF-associated loci by detecting
203 regulatory variants using STARR-seq[14]. We compared these variants with our fine-mapped
204 variants (Supplementary Table 4). Among the 9 loci where fine-mapping identifies one variant at
205 PIP > 0.5, the fine-mapped variants agree with allele-specific variants from STARR-seq in two
206 loci. In the remaining cases, the disagreement is driven by two sources. Most of the allele-specific
207 variants from STARR-seq have much lower GWAS association than fine-mapped variants,
208 suggesting that statistically they are unlikely to be causal variants (see examples in Extended Data
209 Fig. 10). Also STARR-seq tested variant functions *in vitro,* and a few of allelic variants have no
210 regulatory annotations *in vivo* (Supplementary Table 4). These results together added to the
211 emerging picture that in a trait-associated locus, multiple variants may show regulatory effects *in*
212 *vitro*[41]. But to identify true causal variants, we believe one should consider both regulatory
213 information and the strength of GWAS evidence.
214 The fine-mapping results inform how the risk variants are partitioned into various functional
215 categories, such as exons and OCRs in different cell types. The sum of PIPs of all SNPs assigned
216 to a category can be interpreted as the expected number of causal variants in that category. We
217 found that >50% of causal signals are from OCRs and 30% of signals from CM-specific OCRs,
218 highlighting the key role of CMs in AF (Fig. 4f). As expected, exons and UTRs explain only 3%
219 of causal signals.
220 The same PIP summation approach can also be applied to each locus, with the PIP sum of a
221 functional category, e.g., OCRs or exons, now interpreted as the probability that the causal variant

222 in that locus falls into that category. Using this approach, we estimate that at more than half of all
223 loci, causal variants have >50% probability to localize to OCRs (Fig. 4g). Further partitioning of
224 OCRs into cell-type-level categories (Fig. 3b), we identified 37 loci where the causal signals
225 almost entirely (>90%) come from CM-OCRs (Fig. 4h). With the only exceptions of two loci, CM
226 OCRs explain the causal signals in most of the loci, based on OCR annotations (Fig. 4h,
227 Supplementary Table 5). Together these results highlighted that our approach can identify cell type
228 contexts of individual loci.
229
230 **Fine-mapped variants are supported by regulatory annotations and experimental validation.**
231 We characterized the regulatory functions of 68 specific variants at PIP >= 0.5. The majority
232 (42/68) were located in CM-OCRs (Fig. 4i, Supplementary Table 3). 60% (41/68) of all variants
233 and 86% (36/42) of variants in CM-OCRs overlapped H3K27ac marks in the heart, suggesting
234 enhancer activities (Fig. 4i). 40% of variants (27/68) overlapped with fetal DHS[12], suggesting that
235 these variants may act across fetal and adult stages (Fig. 4i). Additionally, 22% of variants were
236 linked to promoters through chromatin loops in Promoter-capture HiC (PC-HiC) from iPSC
237 derived CMs[42] (Fig. 4i). Using mouse ChIP-seq datasets of three key cardiac TFs (*GATA4, TBX5,*
238 *NKX2-5*)[33], we found that five candidate variants are located in human orthologous regions of TF
239 binding sites, representing 4-fold enrichment over expectation by chance (Extended Data Fig. 9e).
240 We also found that 22% (15/68) SNPs alter binding motifs (Fig. 4i) of one of the 76 TFs we
241 identified as likely transcriptional regulators in heart cell types (Fig. 3e). Together, these results
242 supported regulatory functions of many fine-mapped variants.
243 We experimentally tested six non-exonic variants with PIP > 0.95 that were located inside CM-
244 OCRs and overlapped with putative enhancers marked by H3K27ac or H3K4me1/3 (Fig. 4j,
245 Supplementary Table 6). Four out of six variant-containing OCRs induced reporter gene
246 expression in mouse cardiac cells (HL-1 cell line)[43,44] (Extended Data Fig. 11a, Methods), but not
247 in a fibroblast line (3T3), suggesting cell-type-specific activity of the four OCRs (Extended Data
248 Fig. 11b). Three out of these four variants showed allelic changes of reporter activities in cardiac
249 cells, for at least one alternative allele (Fig. 4j). The most striking effect was observed for
250 rs7172038. Two alternative alleles of this SNP (A and G) strongly reduced activation. The
251 enhancer containing this SNP interacts with the promoter of *HCN4* located about 5 kb away,
252 according to Activity-by-Contact (ABC) score[39] (Supplementary Table 3). *HCN4* is a well-known

253 AF risk gene and is physiologically implicated in cardiac rhythm control[45]. Consistent with these
254 results, deletion of a syntenic 20 kb region in mice containing this enhancer significantly reduced
255 the expression of *HCN4*[14]. Notably, in two out of three SNPs with allelic effects, the use of
256 functional information in fine-mapping significantly boosted their PIPs to >= 0.95 (PIP = 0.40 for
257 rs7172038 and 0.41 for rs1152591 under the uniform prior). These experimental results supported
258 regulatory functions of our high confidence variants.
259 In principle, we expect regulatory variants to affect transcript levels of target genes. Using GTEx
260 eQTL data from the left ventricle (LV), we found that only 31% (21/68) variants are eQTLs
261 (Supplementary Table 7). And only in four cases, the eQTLs showed plausible evidence of
262 colocalization (PP4 > 0.5 using coloc[46]) with the AF risk (Supplementary Table 7). The small
263 overlap of fine-mapped variants with heart eQTLs suggests a limitation of bulk eQTL data to
264 identify regulatory variants, an issue we will address in more detail below.
265
266 **A novel computational procedure utilizes fine-mapping results to identify AF risk genes.**
267 Despite our fine-mapping efforts, there remained considerable uncertainty of causal variants in
268 most loci (Fig. 4d). Even if the causal variants are known, assigning target genes can be difficult
269 due to long-range regulation of enhancers[47]. We developed a novel procedure, called Mapgen, to
270 address these problems (Fig. 5a, top): **(1)** For every putative causal SNP, we assign a weight to
271 each nearby gene, considering multiple ways the SNP may affect a gene (see below). The weight
272 of a gene can be viewed as the probability that the SNP affects that gene. **(2)** For each gene, we
273 then aggregate the causal evidence of all SNPs likely targeting this gene, expressed as the weighted
274 sum of the PIPs of all these SNPs. To ensure that the causal evidence of a variant is not counted
275 multiple times when it targets multiple genes, we normalize the SNP-to-gene weights in this
276 calculation. The resulting "gene PIP" approximates the probability of a gene being causal
277 (Methods). Similar to variant-level fine-mapping, we also define a "credible gene set", the set of
278 genes that capture the causal signal at a locus with high probability (Methods).
279 The weights of SNP-gene pairs reflect the strength of biological evidence linking SNPs to genes
280 (Fig. 5a, bottom). For a SNP in an exon or in a regulatory region linked to a particular gene, we
281 assign a weight of 1 to that gene. When a SNP cannot be linked to any gene in these ways, its
282 target genes are assigned using a distance weighted function so that nearby genes receive higher
283 weights (Methods).

284 We identified 46 genes with gene PIP >= 0.8, and 87 with gene PIP >= 0.5 (Fig. 5b,
285 Supplementary Table 8, and Table 1 for top prioritized genes). At each locus, we obtained credible
286 gene sets that captured at least 80% of the causal signal. These credible gene sets contained a single
287 gene in 42 out of 122 blocks, and two genes in 34 blocks (Fig. 5c, Supplementary Table 9). The
288 genes at PIP >= 0.8 included many known AF risk genes such as TFs involved in cardiac
289 development and atrial rhythm control (e.g. *TBX5*[40] and *PITX2*[48]), ion channels (e.g. *KCNN3*[50]),
290 and genes involved in muscle contraction (e.g. *TTN*).
291 We note that a key benefit of Mapgen is that even in the absence of high-confidence causal
292 variants, it may still identify putative risk genes. In 14 out of 46 genes at PIP >= 0.8, the SNP
293 level PIPs were diffused, i.e., no single SNP reached PIP >= 0.5 (Supplementary Table 8). As an
294 example, GJA5, a known AF risk gene[51], was supported by seven SNPs (highest PIP = 0.22), five
295 of which were linked to GJA5 by PC-HiC loops. This led to the gene PIP of 0.80 for GJA5 (Fig.
296 5d, Supplementary Table 3). NKX2-5, a well known transcription factor important for heart
297 development[52], was supported by four SNPs (highest PIP = 0.37), all likely targeting NKX2-5.
298 This led to a gene level PIP = 0.99 (Extended Data Fig. 12, Supplementary Table 3). These
299 examples highlighted the advantage of aggregating information from all putative causal variants.
300 We benchmarked the performance of Mapgen to nominate risk genes against alternative
301 methods. Given the absence of a comprehensive list of known AF risk genes, we used, as a proxy,
302 a set of Gene Ontology (GO) terms previously linked to AF[5]. A gene annotated with one or more
303 of these terms would be considered as a "true" gene in our evaluation, and otherwise a "false"
304 gene. We considered several methods: nearest gene to GWAS lead SNPs (nearest), Activity-by-
305 contact (ABC) score linking enhancers to promoters (ABC-max), a gene association test method
306 (MAGMA), and heart eQTLs linking variants to genes. Additionally, we included a recent study
307 that nominated risk genes in AF-associated loci based on functional genomic data in heart (denoted
308 as van Ouwerkerk[13]). We found that all these alternative methods, except ABC, have precision
309 below or near 50% (Fig. 5e). ABC score has a precision at 60%, but its sensitivity is low, detecting
310 only a few genes. Mapgen, at the threshold of gene PIP > 0.8, reaches a precision of 76%, while
311 detecting nearly 50 genes. These results thus demonstrated the advantages of Mapgen for risk gene
312 discovery.
313 We next examined specific loci in detail to gain insights of the weaknesses of existing methods,
314 and how Mapgen addresses them. We focused on the three commonly used methods, nearest gene

315 method, the use of chromatin interaction data, and eQTL. Among the 46 genes at PIP >= 0.8, eight
316 (17%) were not the nearest genes, by distance to TSS, to the top GWAS SNPs. Some of these
317 genes have been implicated in AF and related phenotypes, including KCNN3, TTN and HCN4.
318 Most of the other genes have plausible functions such as CALU[53], SSPN, and PKP2
319 (Supplementary Table 11). Most of the nearest genes in these loci, in contrast, showed limited or
320 no functional relevance (Supplementary Table 11). As an example, in the locus containing CALU,
321 the nearest gene of the top SNP, rs55985730 (PIP 0.91) is OPN1SW, an opsin gene with function
322 in color vision, but no clear relevance to AF. This SNP is looped to a distal gene CALU in PC-
323 HiC data (Fig. 5f), allowing Mapgen to identify CALU as the likely risk gene. CALU is a calcium-
324 binding protein and involved in alleviation of endoplasmic reticulum (ER) stress in
325 cardiomyocytes[54]. ER stress has a critical role in the pathophysiology of AF[55]. These results
326 suggest that by using chromatin loop information, Mapgen is able to identify distal risk genes.
327 We also considered the use of chromatin conformation in resolving target genes of high PIP
328 SNPs. We found that while chromatin looping data were useful, as shown in the *CALU* example
329 above, using such information alone may miss many potential risk genes. Among 68 SNPs at
330 PIP >= 0.5, only five showed chromatin interactions with promoters based on ABC scores[39], and
331 18 if we included both ABC and PC-HiC data. Additionally, it is common to observe multiple
332 chromatin loops at a single SNP. Among the 18 SNPs with chromatin interactions, 50% (9/18)
333 contact more than one promoter (Supplementary Table 3), highlighting the uncertainty of target
334 genes from chromatin looping data.
335 Use of expression QTLs is another common strategy for linking SNPs to genes. However, as
336 reported above, few fine-mapped variants colocalized with eQTLs. Even if a GWAS SNP is also
337 an eQTL, it may not identify the correct target gene. For example, in the *TTN* locus, the top SNP
338 (rs3731746) is an eQTL of *FKBP7*, but the true risk gene is very likely *TTN*[56,57].
339 Altogether, these results demonstrated the improved ability of Mapgen to nominate plausible
340 candidate genes compared to alternative approaches linking SNPs to genes.
341
342 **Putative AF risk genes are supported by multiple lines of evidence.** We evaluated our candidate
343 genes using multiple sources of data. Consistent with enrichment of AF variants in CM-OCRs,
344 candidate genes (PIP >= 0.8) tended to have higher expression in CMs, compared with other genes
345 in the AF-associated loci (Fig. 6a). Among 46 loci with PIP proportion >= 50% in cardiomyocyte

346 OCR, the likely target genes (gene PIP >= 0.5) were highly enriched (nearly 10-fold) in
347 cardiomyocyte differentially expressed genes (Extended Data Fig. 13a). Additionally, high PIP
348 genes were enriched in AF-related Mendelian disorders (Supplementary Table 12) (Fig. 6b). We
349 also compared our genes with those prioritized by earlier work that used additional functional data
350 such as AF-related gene ontology and heart gene expression[5,13]. While such functional data was
351 not used in our analysis, the genes at PIP >= 0.8 scored on average substantially higher in two
352 earlier studies than low PIP genes (Extended Data Fig. 13b), and 32 of them (71%) were supported
353 by at least one study (Supplementary Table 8).

354 We next assessed the functions of candidate genes using Gene Ontology (GO) and gene
355 networks[58]. GO analysis showed enrichment of Biological Processes related to heart development
356 and cardiac function, and of Molecular Functions such as ion channels, hormone binding and
357 protein tyrosine kinase (Fig. 6c, Supplementary Table 13). For network analysis, we used the
358 STRING gene network built with genes at a relaxed PIP threshold of 0.5 (87 genes) to increase the
359 number of interactions. This analysis highlighted some well-known processes in AF, such as ion
360 channels, and structure components of heart muscle (Fig. 6d). A prominent subnetwork consisted
361 of key TFs, including *GATA4, TBX5, NKX2-5* and *HAND2*, implicated previously in AF genetics
362 and/or heart development[40,59–61] (Fig. 6d). Two other TFs in the network, *PITX2* and *ZFHX3*, are
363 also well-known AF genes[40]. Combined with the fact that putative causal variants were enriched
364 in binding sites of TBX5, NKX2-5 and GATA4 (Fig. 4i, Extended Data Fig. 9e), these results
365 suggested that perturbation of transcriptional regulatory networks consisting of TFs and their
366 targets, plays a critical role in the genetics of AF. Additionally, the interaction network highlighted
367 signal transduction pathways, including MAPK signaling and Ephrin signaling (Fig. 6d). Both
368 processes are important in heart development[62–65]. Indeed, 19 out of 87 genes at PIP >= 0.5 were
369 annotated by the GO term "regulation of intracellular signal transduction" (FDR < 0.02)
370 (Supplementary Table 14).

371 Finally, we found additional literature support for the candidate genes. 39 out of 46 (85%) genes
372 at PIP >= 0.8 have reported roles in cardiac processes and/or diseases from literature
373 (Supplementary Table 10). The subset of genes at PIP >= 0.95 with literature support, as well as
374 their supporting SNPs, were shown in Table 1. The majority of these genes have not been
375 established as AF risk genes through functional studies, representing novel yet biologically
376 plausible risk genes.

377

378 **Cell-type-specific epigenomes reveal insights to lack of colocalization of GWAS signals to**
379 **heart eQTLs.** While a large fraction of fine-mapped AF SNPs fell inside CM-specific OCRs (Fig.
380 4f), most of them did not colocalize with heart eQTLs (Supplementary Table 7). This result adds
381 to the growing evidence that eQTLs may explain a relatively small percent of GWAS signals of
382 complex traits[66,67]. It is unclear, however, why this is the case[68]. We took advantage of our cell-
383 type resolved transcriptomic and epigenomic data to investigate this issue. We hypothesized that
384 the heart eQTLs missed a large fraction of regulatory variants specific to CMs, thus were depleted
385 of AF risk variants. To assess this hypothesis, we focused on 1,216 heart (LV) eQTLs from GTEx
386 where the causal variants (known as eQTNs) were fine-mapped with high confidence (PIP >= 0.8)
387 (Supplementary Table 15).
388
389 Given that the heart eQTL study was performed on bulk tissues, the cell types where these eQTLs
390 act are unknown. We used eQTL information in other tissues to infer whether the eQTLs are likely
391 CM-specific. Our reasoning is that eQTLs that were found across many tissues are likely to be
392 functional in cell types shared across tissues, thus not specific to CMs. We found that the majority
393 of eQTLs were highly shared, i.e., found in >30 tissues in GTEx (Fig. 7a). Less than 10% of heart
394 eQTLs were found in 5 or fewer tissues. These results thus suggest that the detected heart eQTLs
395 are highly biased towards variants with effects in cell types shared across tissues.
396
397 This finding thus confirms our hypothesis that the detected heart eQTLs are generally not specific
398 to CMs, even though CMs constitute a relatively large fraction of heart cells (20-30%, Fig. 2a). To
399 understand these results, we divided the heart eQTLs into different categories based on the location
400 of the eQTNs, including exons, UTRs, introns, OCRs in specific cell types, and OCRs shared with
401 varying numbers of cell types. We analyzed the tissue-sharing pattern of each category separately.
402 The overall sharing pattern of all eQTLs would depend on the sharing pattern of each category,
403 and the percent of eQTLs in each category (see Methods). This analysis would thus allow us to
404 understand what drives the high degree of observed eQTL sharing across tissues.
405
406 As expected, eQTLs falling into OCRs shared in multiple cell types were extensively shared across
407 tissues (Fig. 7b). On the other hand, eQTLs in cell-type-specific OCRs showed variable levels of

408 sharing. Fibroblast-eQTLs (eQTLs in fibroblast-specific OCRs) and myeloid-eQTLs were highly
409 shared (median 31 and 43 tissues, respectively), but most CM-eQTLs were found in <10 tissues
410 (Fig. 7b). We believed this variability reflected different degrees of cell type sharing between the
411 heart and other tissues. To test this, we compared heart eQTLs with those from the brain and whole
412 blood. As expected, heart eQTLs from immune cell OCRs had the highest sharing with whole
413 blood, while eQTLs of all heart cell types have low sharing with the brain (Fig. 7c). Together,
414 these results highlighted considerable variability of tissue sharing patterns of heart eQTLs,
415 depending on their likely cell-type origins.
416
417 We next assessed the proportions of heart eQTLs in functional categories, focusing on eQTLs in
418 OCRs, whose cell type origins could be inferred. A large proportion of those eQTLs were from
419 OCRs shared in multiple cell types, with eQTLs in CM-specific OCRs only explain <10% of heart
420 eQTLs (Fig. 7d). Given that different categories of OCRs have different genome sizes, we
421 compared the proportions of eQTLs in each category with random expectation (Methods). While
422 eQTLs in OCRs from single cell types showed 2-9 fold enrichment, those shared with 4 or more
423 cell types showed 26-fold enrichment (Fig. 7d). Indeed, the enrichment is highly correlated with
424 the number of cell types in which an OCR is detected (Fig. 7e). We thus concluded that discovered
425 eQTLs are biased towards those with broad effects across multiple cell types.
426
427 Altogether, our results suggest that eQTLs that are likely CM-specific are under-represented in the
428 data, constituting <10% of all heart eQTLs. Most of the remaining eQTLs have effects across
429 multiple cell types; or have effects in cell types shared across other tissues. As a result, the overall
430 level of tissue sharing of heart eQTLs is very high. Given that AF risk variants are specifically
431 enriched in CM-specific OCRs (Fig. 4a), the depletion of CM-specific eQTLs explains why heart
432 eQTL data fail to explain most GWAS signals.
433
434 We reason that this depletion of cell-type-specific regulatory variants in eQTLs can be explained
435 by the nature of bulk eQTL studies. When the effect of an eQTL on a gene is limited to a single
436 cell type, but the gene is expressed in other cell types, the effect of the variant on the bulk gene
437 expression would be diluted, leading to lower power of detecting this eQTL. This argument was
438 supported by the observation that gene expression was less cell-type-specific than accessibility of

439 regulatory elements. In heart eQTLs localized to CM-specific OCRs, the expression of
440 corresponding genes in CMs were only modestly higher than their expression in other cell types
441 (Extended Data Fig. 14a). We performed simulations to investigate the power loss in detecting
442 cell-type-specific eQTLs. When the cell type of interest is 20% of the bulk tissue, we estimate that
443 the power of detecting eQTL specific in this cell type is only about 8-40% of the power of detecting
444 eQTLs with shared effects across cell types (Supplementary Notes, Extended Data Fig. 14b). This
445 analysis demonstrated that the low power of detecting cell-type specific eQTLs is a key limitation
446 of bulk eQTL studies.
447
448 **Discussion**
449 While GWAS have been successful in a range of complex traits, the causal variants, their target
450 genes, and their mechanisms in disease-related cell types have been elucidated in few cases[47]. In
451 this work, we established a cell-type-resolved atlas of chromatin accessibility and transcription of
452 the human heart to study the genetics of heart-related traits, focusing on AF[3–5]. We statistically
453 fine-mapped AF-associated loci, and experimentally validated some of the candidate variants.
454 Using a novel computational procedure, we identified 46 high confidence genes, implicating key
455 biological processes, in particular TFs and signaling pathways important for heart development.
456 Motivated by our observation that the putative AF variants often were not colocalized with eQTLs,
457 we investigated how heart eQTLs are shared across tissue types. Our analysis suggests that eQTLs
458 with cell-type-specific effects are under-detected and that this is likely a factor explaining both
459 high tissue-sharing of eQTLs and the lack of eQTLs in GWAS variants.
460 Compared with several recent studies that aimed to identify risk variants and genes in AF[13,15],
461 our study has a few key advantages. Hocker *et al*. intersected fine-mapped variants with cell-type-
462 resolved OCRs to nominate putative regulatory variants. Their work and related studies[69]
463 demonstrated the utility of single cell ATAC-seq data for interpretation of non-coding variants
464 from GWAS. Our work extends these studies by using a computational procedure that leverages
465 the strong enrichment of genetic signals in CM-specific OCRs to fine-map causal variants,
466 identifying 68 high confidence SNPs at PIP > 0.5, including 42 in CM OCRs, compared to five
467 nominated by Hocker *et al.*[15] (Fig. 4b). Our gene-mapping procedure effectively leverages fine-
468 mapping results and multiple sources of information linking SNPs to putative targets. This avoids
469 the bias of previous work that only considers one metric, e.g., distance, to link SNPs to genes, and

470 increases the sensitivity of detecting risk genes. As a result, we found high confidence genes
471 (PIP >= 0.8) in more than 1/3 of known AF-associated loci.
472 Our set of 46 candidate genes shed light on the genetics of AF. Earlier linkage studies implicated
473 ion channels and structural proteins, as well as a few TFs[70]. Our results confirmed these earlier
474 findings and showed an even larger role of regulatory genes, including TFs and signaling proteins.
475 In total, we identified 13 TFs with PIP >= 0.8 (Supplementary Table 10), and 18 at PIP >= 0.5.
476 These included known AF genes, TBX5 (PIP 0.99), NKX2-5 (0.99), PITX2 (0.99), ZFHX3 (0.85)
477 and GATA4 (0.57), as well as TFs with roles in heart development such as HAND2 (0.87), ZEB2
478 (0.98), and PRRX1 (0.72). Our results also highlighted signal transduction pathways, including
479 MAPK signaling[62], Ephrin signaling[63–65] (Fig. 6d), G-protein coupled receptor signaling[71], Wnt
480 signaling[72] (Supplementary Table 13) and FGF signaling[73,74] (FGF9, PIP = 0.94 and FGF5 PIP =
481 0.53), all previously implicated in heart development.
482 Despite the advances described above, our study has a few limitations. Our experimental data
483 were limited to four anatomical locations of the ventricles, while some AF risk variants might act
484 through atrial-specific CMs. However, it is worth noting that a recent study, using scRNA-seq
485 based cellular atlas of the heart including all anatomic locations, found that AF candidate genes
486 were strongly enriched in ventricular CMs[17]. Additionally, our fine-mapping leveraged the almost
487 exclusive enrichment in CM-specific OCRs (Fig. 4a), and thus may miss variants acting on the AF
488 risk through other cell types. This possibility is suggested by a small number of candidate variants
489 showing accessibility specific to fibroblasts (Fig. 4h), known contributors to AF etiology[75].
490 Finally, some disease variants potentially act transiently during development and might be missed
491 using adult heart samples.
492 In conclusion, by combining novel experimental and computational approaches, our study
493 identified a number of risk variants and genes and revealed key insights of the genetics of AF.
494 These data provide a rich resource for future functional studies. Importantly, our analytic
495 framework, including the software for fine-mapping and risk gene identification, may provide a
496 general model for the study of other complex phenotypes.
497
498 **Methods**
499

500 **Data collection.** *Nuclei isolation from adult heart tissue.* Heart tissue samples were obtained from
501 National Disease Research Interchange (NDRI) and were stored at -80ºC and kept on dry ice
502 whenever outside of the freezer. We included samples from 4 regions (left and right ventricles,
503 interventricular septum, apex) from 3 male individuals (Supplementary Table 1). Aliquots of each
504 heart sample were prepared from frozen heart tissue using a tissue pulverizer, which was cooled
505 prior to pulverization for 20 minutes over dry ice. Aliquots assayed in this study ranged from 86.7
506 mg to 141.6 mg. Prior to library preparation, we purified nuclei using fluorescence-activated cell
507 sorting (FACS) to remove debris and minimize contamination from ambient RNA.
508 Single nuclei isolation was performed on the heart tissue aliquots as described in Litvinukova
509 *et al.* 2020[17], with some modifications. Single heart aliquots were kept on dry ice until being
510 transferred into a precooled 2 mL dounce homogenizer (Sigma) with 2 mL homogenization buffer
511 (250 mM sucrose, 25 mM KCl, 5 mM MgCl2, 10 mM Tris-HCl, 1 mM dithiothreitol (DTT), 1x
512 protease inhibitor, 0.4 U/µl, RNaseIn, 0.2 U/µl SUPERaseIn, 0.1% Triton X-100 in nuclease-free
513 water). Samples were dounced 25 times with pestle A (loose) and 15 times with pestle B (tight),
514 filtered through a 40-µm cell strainer, and centrifuged (500g, 5 minutes, 4ºC). Supernatant was
515 discarded and the nuclei pellet was suspended in nuclei resuspension buffer (1x PBS, 1% BSA,
516 0.2 U/µL RnaseIn) and stained with NucBlue Live ReadyProbes Reagents (ThermoFisher).
517 Hoechst-positive nuclei were enriched using fluorescence-activated cell sorting (FACS) on the
518 FACSAria (BD Biosciences), obtaining between 172,500 and 350,000 nuclei while targeting a
519 maximum of 350,000. Nuclei were sorted into 0.75 ml of resuspension buffer. Flow-sorted nuclei
520 were counted in a C-Chip Disposable Hemocytometer, Neubauer Improved (INCYTO) before
521 commencing with library preparation.
522
523 *snRNA-seq library preparation and sequencing*. A portion of the sorted nuclei suspension was
524 removed and brought to a concentration of between 700 and 1,200 nuclei per microliter. An
525 appropriate number of nuclei were loaded on the Chromium controller (10X genomics) in order to
526 target between 6,000-8,000 nuclei, according to V3 of the manufacturer's instructions for the
527 Chromium Next GEM Single Cell 3′ Reagent Kits (10X Genomics)[76]. 3' gene expression libraries
528 were amplified with 15 cycles during sample index PCR. QC was performed on 3' gene expression
529 cDNA and final libraries using a Qubit Fluorometer (ThermoFisher) and an Agilent 2100

530 Bioanalyzer (Agilent). Libraries were sequenced on the NovaSeq 6000 (Illumina) or the NextSeq
531 500 (Illumina) at the University of Chicago's Genomics Facility using paired-end sequencing.
532
533 *scATAC-seq library preparation and sequencing*. scATAC-seq libraries were prepared according
534 to v1 of the manufacturer's guidelines for the Chromium Next GEM Single Cell ATAC Reagent
535 Kits (10X Genomics), with the modification that we started from nuclei that were isolated as
536 described above. Between 9,300 and 25,000 nuclei were tagmented using Transposition Mix (10X
537 Genomics) at 37°C for 1 h and loaded on the Chromium controller. We targeted between 6,000
538 and 10,000 nuclei for library preparation. QC was performed on final ATAC-seq libraries using a
539 Qubit Fluorometer and an Agilent 2100 Bioanalyzer. Libraries were sequenced on the
540 NovaSeq6000 or the NextSeq500 at the University of Chicago's Genomics Facility using paired-
541 end sequencing.
542
543 **Single-cell genomic data analysis.** *snRNA-seq pre-processing.* FastQ files from 12 sequencing
544 experiments were individually processed using an in-house scRNA-seq pipeline dropRunner[77].
545 Briefly, dropRunner utilizes FastQC[78,79] to obtain quality control metrics followed by fast and
546 efficient alignment to human reference genome hg38 using `STARsolo 2.6.1`[80] in `GeneFull`
547 mode with other parameters set to default. STARsolo performs alignment and quantification of
548 gene expression in one package. We quantified expression at the gene level using `Gencode v29`
549 gene annotations[81] utilizing both intronic and exonic reads to improve clustering and downstream
550 analyses of the snRNA-seq data. We extracted the raw gene-by-barcode expression matrices output
551 by STARsolo for downstream analyses. We used `Seurat 3.2.1`[82] in R to analyze the snRNA-
552 seq data. We combined all 12 expression matrices into a single Seurat object together with the
553 corresponding metadata such as donor and anatomical region. To filter low-quality nuclei, we
554 removed barcodes that contained less than 1000 UMI. We also used `DoubletFinder 2.0.3`[83]
555 with `pN = 0.015` and `pK = 0.005` to account for doublets, which works by generating in-
556 silico doublets and performs clustering to identify nuclei that fall in the neighborhood of the
557 generated doublets. After quality control, we retained a total of 49,359 nuclei.
558
559 *scATAC-seq pre-processing.* FastQ files from 12 sequencing experiments were individually
560 processed using 10x Genomics `CellRanger-atac 1.2.0`[84]. We used the command

561 `cellranger-atac count` to align the fastq files to human reference genome hg38, followed by
562 marking and removing duplicate reads, and producing a fragment file containing the mapped
563 location of each unique fragment in each nucleus. We used `ArchR 0.9.5`[29] to further pre-process
564 the data and perform downstream analyses of the scATAC-seq data. Using ArchR, we converted
565 the fragments file into a tile matrix, which is a bin-by-barcode Tn5 insertion count matrix, using a
566 bin-size of 500 bp. We also generated a gene score count matrix using the "model 42" from ArchR,
567 which aggregates Tn5 insertion signals from the entire gene body, scales signals with bi-directional
568 exponential decays from the TSS (extended upstream by 5 kb) and the transcription termination
569 site, and accounts for neighboring gene boundaries. Gene annotations were obtained from
570 `Gencode v29`. To filter low quality nuclei, we kept nuclei with at least 5,000 unique fragments
571 and a TSS enrichment score of 6. We also used ArchR's doublet removal approach with default
572 parameters, which is based on in-silico doublet generation. We removed nuclei with a doublet
573 enrichment score greater than 1. After quality control, we retained a total of 26,714 nuclei.
574
575 *Cell-type identification from snRNA-seq and scATAC-seq.* We performed normalization,
576 dimensionality reduction, and unsupervised clustering on snRNA-seq and scATAC-seq data in
577 order to identify cell-types. For snRNA-seq, we used Seurat's workflow which begins with
578 converting counts to log2 TP10k values using the `NormalizeData` function. Next, we found the
579 top 2000 variable genes using `FindVariableGenes` and used these genes as input features for
580 Principal Component Analysis (PCA). We computed the top 30 principal components (PCs) for
581 each cell and used these for downstream analyses. We observed batch effects due to different
582 donors, and corrected this batch effect. This was done using the `RunHarmony` function from the
583 `Harmony 1.0`[85] package with default parameters to regress out the donor variable from the PCs.
584 Next, we used the `FindClusters` in Seurat with a resolution of 0.2 on the harmony-corrected
585 PCs to define clusters. We also computed the corresponding UMAP to visualize the harmony-
586 corrected PCs in two dimensions. We used previously established cell-type markers in order to
587 map clusters to cell types[17,18].
588 We performed cell-type mapping for scATAC-seq using the `ArchR` package. We performed
589 dimensionality reduction on the tile matrix using the top 20,000 bins in terms of count across all
590 cells. We used the function `addIterativeLSI` with 2 iterations in order to perform latent
591 semantic indexing (LSI) on the scATAC-seq tile matrix and retained the top 50 LSI vectors.

592 Similar to snRNA-seq, we observed batch effects across different donors, and removed this effect
593 using the `RunHarmony` function. We used `addClusters` with `resolution = 0.2` in order to
594 cluster nuclei based on the harmony-corrected LSI vectors. `addUMAP` with `min.dist = 0.4` was
595 used to compute a 2-dimensional representation of the harmony-corrected LSI vectors. We
596 visualized gene activity scores, as defined in ArchR, using the same marker genes as in snRNA-
597 seq to assign clusters to cell-types.
598
599 **Defining and classifying open chromatin regions**. Insertion read counts were aggregated across
600 all cells in each cell-type to form a cell-type pseudo-bulk and peak calling was performed on
601 pseudo-bulk data of each cell-type. Using the function `addReproduciblePeakSet` in ArchR in
602 conjunction with MACS2[86], a union set of 352,900 peaks were called in total across all cell-types
603 at FDR < 0.1. This set of peaks, called union set, were used for all downstream analyses.
604 In order to discover cell-type specific regulatory elements, a single-cell insertion count matrix
605 was created using the function `addPeakMatrix` in ArchR. Cells were grouped into their
606 respective cell-types and differential accessibility (DA) analysis was performed in a one-vs-all
607 fashion, i.e., one cell type vs. all other ones. To perform DA, we used `getMarkerFeatures` in
608 ArchR with default parameters, which uses the Wilcoxon rank-sum test on the log-normalized
609 insertion count matrix. To control for technical variation, cells from the cell-type group and the
610 group of remaining cell types are matched in terms of TSS enrichment and number of fragments.
611 Using FDR < 10% and $\log_2$ fold-change > 1, we found about 47% of the union set to be cell-type
612 specific.
613 For OCRs that were not differentially accessible, we reasoned that these are more likely to be
614 shared. To further stratify these OCRs into different classes, based on sharing among different cell
615 types, we used a simple quantile-based method. First, we aggregated the ATAC-seq counts across
616 all cells within each cell-type for each non-DA peak and normalized the counts by the total sum
617 of counts in each cell-type. Next, we binarized the peaks within each cell-type based on whether
618 they are in the top 25% or not in terms of their normalized counts. In this way, we identify the top
619 25% accessible peaks in each cell-type. Finally, we count how many times a peak is 1, or highly
620 accessible, across cell-types. Through this strategy, we defined three disjoint sets: shared in 2-3
621 cell types, shared in 4+ cell types and the remaining peaks denoted as "non-DA". The last category

corresponds to peaks that are only highly accessible (top 25%) in one cell type but are not found to be differentially accessible based on our criteria above.

Comparing snRNA-seq and scATAC-seq. We calculated correlation scores of gene expressions from snRNA-seq and gene activities from scATAC-seq in the following manner: First, we selected genes that were up-regulated in each cell type according to differential expression analysis of snRNA-seq data. Approximately 3000 genes were identified in this manner. For each gene, the ATAC-seq gene scores and RNA-seq transcript counts, respectively, were aggregated across all cells in each cell-type cluster, followed by a log transformation. We then used the log-transformed pseudo-bulk gene scores and normalized expression levels to calculate Pearson correlation between gene scores and expression across cell types.

Comparing the cell labels in our study with Litviňuková's et al. Label transfer was performed using Seurat to compare the labels in our study with Litviňuková's *et al.* [17]. The processed scRNA-seq data from Litviňuková *et al.* were downloaded from `https://www.heartcellatlas.org/#DataSources`. `LoadH5Seurat` from `Seurat` R package was used to convert the h5ad format into a Seraut object. Next, anchors were identified using the `FindIntegrationAnchors` function and used as reference, which takes the earlier Seurat object as input. Then, we predicted the labels of our cells with the `TransferData` function, which used the anchors and our scRNA-seq data (also a Seurat object) as inputs and returned the predicted labels for each cell in our dataset. We summarized the number of matched cells with a heatmap, showing the proportion of matched cells in each cluster.

Comparing the OCRs in our study with Hocker et al. We compared the OCRs from our dataset with Hocker *et al.*[15] using peak sets called on individual cell type clusters. Cell-type level peaks identified by Hocker *et al.* were obtained from their CARE portal (`http://cepigenomics.org/CARE_portal/Cell_Type_Diversity.html`). We only included their peak set from ventricular CMs to match our cell types. For each cell type, we computed a simple overlap between peaks from both datasets using `GenomicRanges` `findOverlaps`[87] in R. Overlaps for each cell type were represented as Venn diagrams generated with the `eulerr` R package.

653

654 **Identifying putative TFs regulating chromatin accessibility.** We used a set of 870 human motif
655 sequence instances from `CisBP`[88]. These motif annotations were added onto the ArchR object
656 using the `addMotifAnnotations` function. Next, enrichment analysis was performed for each
657 motif in each cell-type-specific set of peaks, using the `peakAnnoEnrichment` function in ArchR.
658 The function uses the hypergeometric test to assess the enrichment of the number of times a motif
659 overlaps with a given set of peaks, compared to random expectation. After correcting for multiple
660 testing within each cell-type, we used FDR < 1% to ascertain a set of motifs and their enrichment.
661 Motif enrichment analysis may find multiple TFs with similar motifs. To reduce the redundancy
662 and identify true TFs that drive gene regulation, we correlated the motif accessibility with gene
663 score activity of each TF, expecting that for true TFs, their expression levels should be positively
664 correlated with accessibility of their motifs across cells. We obtained motif accessibility scores
665 from `chromVAR`[32] (using the `addDeviationsMatrix` function in ArchR) for each TF across all
666 cells. We obtained the corresponding TF gene activity scores using the "model 42" by ArchR (see
667 "scATAC-seq pre-processing"). These single-cell-level motif accessibility scores and gene scores,
668 however, are noisy given the sparsity of data at individual cells. We thus used a strategy similar to
669 Cicero[89], by aggregating cells into "metacells" based on similarity using a *k*-nearest neighbor
670 approach. Specifically, we found the *k* nearest neighbors to each cell using the LSI vectors of the
671 single-cell ATAC-seq data. We only retained sets of metacells that shared a maximum of 25% of
672 constituting cells. Metacells that shared more than 25% of cells were removed at random. Using *k*
673 = 100, we created about 200 non-redundant meta-cells based on these criteria and averaged the
674 motif accessibility scores and gene scores across cells within each meta-cell. We then computed
675 Pearson's correlation between the gene scores and the motif accessibility scores across meta-cell.
676 We selected all TFs with a Pearson's correlation greater than 0.5.
677

678 **SCAVENGE analysis.** SCAVENGE[36] was used to calculate for each cell a trait relevance score
679 (TRS) for Atrial fibrillation. SCAVENGE was run under default settings, with ATAC-seq peak
680 matrix and fine-mapping results (under the uniform prior) as inputs.
681

682 **Testing enrichment of GWAS risk variants in functional annotations.** We obtained
683 harmonized GWAS summary statistics for cardiovascular and some non-cardiovascular traits from

684 the IEU OpenGWAS project. We removed SNPs with missing values, SNPs on non-autosomal
685 chromosomes, and indels. Utilizing approximately independent Linkage Disequilibrium (LD)
686 blocks generated by ldetect[37], we assigned each SNP to one of 1700 LD blocks.
687 We used TORUS[34] to estimate the genome-wide enrichment of risk variants of GWAS traits in
688 various functional annotations, including cell-type specific OCRs obtained from DA testing, and
689 some generic annotations including coding, retrieved from UCSC Genome Browser database, and
690 conserved sequences from Lindblad-Toh, K. *et al.* 2011[90]. We ran TORUS on each annotation,
691 one at a time, to get the marginal enrichment reported in Fig. 4a. P-values for enrichment were
692 estimated from the 95% confidence intervals returned by TORUS and were adjusted for multiple
693 testing across all traits/cell-types using the Benjamini-Hochberg approach.
694
695 **Fine-mapping causal variants in AF-associated loci**. We start with a general description of
696 statistical fine-mapping analysis. We assume the trait of interest, Y, is related to the genotypes of
697 all variants in a locus by a linear model. Let X_j be the genotype of the j-th variant, we have: $Y =$
698 $\sum_j X_j \beta_j + \epsilon$, where β_j is the effect size of the j-th variant. Because causal variants in a locus are
699 generally "sparse", it is often assumed that most β_j's would be zero. It is easy to see that, under
700 this model, even if a single variant has $\beta_j \neq 0$, other variants in LD with this variant would appear
701 associated with the trait in the standard single-variant association analysis. But in the joint
702 regression model here, once we choose the correct causal variant(s), conditioned on them, the non-
703 causal variants in LD would no longer be associated with the trait. The goal of fine-mapping is
704 then to select as few variants with $\beta_j \neq 0$ as possible to explain all associations in the locus. This
705 "variable selection" step is often accomplished using a Bayesian spike-and-slab prior, which
706 assumes that β_j follows a mixture distribution of point mass at 0, and a normal distribution. The
707 mixture proportion of the point mass is typically very large (close to 1), ensuring that at most a
708 few variants would have non-zero effects. Inference of this model is computationally difficult. We
709 used SuSiE in our analysis [38]. SuSiE uses an efficient variational Bayes procedure, and generally
710 outperforms other fine-mapping tools. The main output of SuSiE is the posterior probability that
711 $\beta_j \neq 0$, denoted as Posterior Inclusion Probability (PIP).
712

713 To run SuSiE on our GWAS summary statistics, we first partitioned the genotype into LD blocks
714 using LDetect[37,38]. Then, we ran the `susie_rss()` function on each LD block. The input of this
715 function includes GWAS z-scores and the LD matrix for the SNPs in a block. The GWAS
716 summary statistics were available publicly. For the LD matrix, we used out-of-sample genotype
717 information from 1000 Genome Project[91]. We ran SuSiE with `L = 1`, which allows a single causal
718 signal for each LD block and is robust to mismatching LD patterns. We fine-mapped a total of 122
719 LD blocks in the AF GWAS, each containing at least 1 SNP at genome-wide significance ($P < 5$
720 $\times 10^{-8}$).
721
722 To incorporate functional information of variants in fine-mapping, we allowed SNPs to have
723 different prior probabilities in SuSiE. Specifically, each SNP has a different prior distribution of
724 β_j, with the prior probability that $\beta_j \neq 0$, denoted as π_j, dependent on the functional information
725 of that SNP. These prior probabilities are estimated using TORUS[21]. Briefly, TORUS assumes that
726 π_j is related to the annotations of the SNP through a logistic regression model. These annotations
727 may include, for example, whether a SNP is located in an OCR in CMs, or in an evolutionarily
728 conserved region. The parameter of an annotation in the model encodes the extent to which causal
729 variants are enriched in this annotation. TORUS uses the entire GWAS data of all variants in the
730 genome to estimate these parameters. We included the following annotations in TORUS: CM
731 specific OCRs, CM shared OCRs, CM non-DA OCRs, non-CM OCRs, UCSC conserved, coding,
732 or finemapped eQTLs.
733
734 **Annotating putative AF causal variants with additional functional data**. Fetal DHS and heart
735 H3K27ac data were obtained from ENCODE. PC-HiC interactions were obtained from an earlier
736 study conducted in iPSC derived CMs[42]. Only interactions found in at least 2 out of 3 replicates
737 were included. Motif analysis was performed using R `motifbreak` package[92] . Only "strong"
738 effects on motif scores, according to the package, were considered.
739
740 **Assessing regulatory effects of candidate variants by Luciferase assay.** Candidate regulatory
741 elements were designed from CM-specific accessibility in hg38 and synthesized by IDT, with
742 either the reference allele or SNP allele(s). Sequence was verified and then cloned into the
743 pGL4.23 enhancer luciferase response vector with a minimal promoter. HL-1 cardiomyocytes

744 were co-transfected with luciferase response vector and a pRL control using Lipofectamine 3000,
745 cultured for 48 hr after transfection, then lysed and assayed using the Dual-Luciferase Reporter
746 Assay system (Promega). For each construct reporter gene activity was assayed in 5 replicates.
747
748 **Gene mapping procedure with Mapgen.** We used the posterior inclusion probabilities (PIPs)
749 generated by SuSiE to calculate a gene-level PIP, reflecting the probability that a gene is a risk
750 gene. We assume there is a single causal gene per disease associated locus. Let Z_g be an indicator
751 variable describing whether gene *g* is causal ($Z_g = 1$) or not ($Z_g = 0$) for the trait. Assuming a single
752 causal SNP per locus, the probability that the gene is causal, which is denoted as "gene PIP", can
753 be then related to the probabilities of SNPs being causal variants:

754 $$P(Z_g = 1 \mid D) = \sum_i P(Z_g = 1 \mid \gamma_i = 1) P(\gamma_i = 1 \mid D),$$

755 where γ_i is the indicator variable for whether SNP *i* is causal or not, and *D* is the GWAS summary
756 statistics. The term $P(Z_g = 1 \mid \gamma_i = 1)$ is the probability that *g* is the causal gene if the causal SNP
757 is SNP *i*, and the term $P(\gamma_i = 1 \mid D)$ is simply the PIP of SNP *i*, or PIP_i. So the gene PIP of a gene
758 is a weighted sum of PIPs of all SNPs, weighted by how much that gene is supported by each SNP
759 (see below). Since the PIPs of all SNPs in a block sum to 1, the gene PIP has an upper-bound of
760 1. In the rare cases where a gene spans two nearby blocks - e.g. when a gene has large introns, the
761 gene PIP may exceed 1, which can be interpreted as the expected number of causal variants
762 targeting the gene *g*.
763 To calculate the term $P(Z_g = 1 \mid \gamma_i = 1)$, we consider the location of the SNP *i* with relation to
764 the gene *g*, as well as functional genomic data linking SNP *i* with gene *g*. These data were used to
765 assign the weights, denoted as w_{ig}, between SNP *i and* gene *g*, reflecting how likely the SNP *i*
766 affects gene *g*. For example, if a SNP is inside an exon of a gene, then the SNP-gene will have
767 weight 1. We note that w_{ig} and $P(Z_g = 1 \mid \gamma_i = 1)$ have different semantics: it is possible that a
768 SNP affects multiple genes with weights all equal to 1, but there is only a single causal gene
769 supported by any SNP. In other words, for a causal SNP *i*, the conditional probabilities $P(Z_g =$
770 $1 \mid \gamma_i = 1)$ should sum to 1 across all nearby genes *g*. So we need to normalize w_{ig} with:

771 $$P(\gamma_i = 1) = \frac{w_{ig}}{\sum_g w_{ig}}$$

772

773 To assign the weight terms, w_{ig}, we follow these four steps capturing several scenarios where a
774 SNP may affect a gene: **1)** If a SNP is in an exon or active promoter (promoter overlapping with
775 OCR) of a gene, we assign the SNP to that gene with weight $w_{ig} = 1$. **2)** If a SNP can be linked
776 to a gene's promoter via "enhancer loops", we assign the linked gene with weight $w_{ig} = 1$. Here,
777 "enhancer loops" are defined based on Activity-By-Contact (ABC) scores (constructed from heart
778 ventricle data with ABC scores >= 0.015)[39] and promoter-capture HiC data (from iPSC-CMs)[42].
779 Considering the fact that Hi-C and PC-HiC may miss contacts between close regions due to
780 technical reasons, we also consider a SNP in OCR within 20 kb of an active promoter as an
781 "enhancer loop". **3)** If a SNP is in a UTR but not in OCRs, suggesting that the SNP likely regulates
782 the containing gene through RNA processing mechanisms, e.g. RNA stability or alternative
783 polyadenylation, we will assign the SNP to the UTR-containing gene with weight $w_{ig} = 1$. **4)** If
784 a SNP is not linked to any gene via the criteria above, we use a distance-based weighting to assign
785 it to all genes within 1Mb. The weights follow an exponential decay function as below, where
786 d_{ig} is the SNP-gene distance:

787 $$w_{ig} = e^{-d_{ig}/5\times10^4}.$$

788 The parameter of this weight function, 50 kb, was chosen based on the fact that most enhancers,
789 estimated to be 84% using CRISPR deletion experiments[93], are located within 100 kb of the target
790 promoters. Using a weight of 50 kb here would lead to 87% of weights within 100 kb, with a
791 simple area-under-curve calculation of the weight function above.

792 At any locus, having PIPs for all the genes in the locus allows us to define the "credible gene
793 set" of the locus, much like the use of the term for SNPs[38]. Simply speaking, the credible set at the
794 80% level means the minimum set of genes in the locus whose sum of PIPs is greater than or equal
795 to 80%. One complication is that some of the genes in the locus may span another nearby locus,
796 as described above. In this case, while the final reported gene PIP is computed from both loci, we
797 only use the PIP of the gene from the locus of interest to define the credible gene set of that locus.
798

799 **Benchmarking performance of different methods for risk gene identification.** We compared
800 the accuracy of Mapgen (gene PIP >= 0.8), and several other commonly used methods that
801 nominate risk genes from GWAS (see below). Given that we do not have a gold standard list of
802 known AF genes, we used a set of Gene Ontology (GO) terms that have been associated with AF

genetics (using DEPICT method) from an earlier study (Nielsen *et al.*[5], Supplementary Table 7). We used FDR < 5% and required three or more genes in a gene set, to select 173 GO terms. We call a candidate gene "plausible", if the gene is annotated with any of those GO terms. Then we compared the precision of the methods, calculated as the number of plausible genes divided by the total number of nominated genes.

We included the following methods in the comparison: (1) Nearest gene to the top GWAS SNP (based on distance to gene TSS). (2) eQTL, linking gene to the top GWAS SNP in each locus using GTEx eQTL from the left ventricle (LV). (3) Activity-by-Contact (ABC) scores, linking promoters with enhancers based on chromatin-looping data. Following Nasser *et al* [39], we used the ABC-max approach, linking each top SNP to the gene with the maximum ABC score. (4) Multi-marker Analysis of GenoMic Annotation (MAGMA), gene association test method[27]. We ran MAGMA gene analysis and identified genes with Bonferroni adjusted p-value < 0.05. (5) In addition to the above methods, we also included the nominated genes (gene score >= 11) from van Ouwerkerk *et al.*[13].

Gene interaction network analysis. We used the STRING database (`STRING 11.5`)[94] to construct gene network. The analysis was done using `Cytoscape 3.8.2`[95]. The input genes are those at PIP >= 0.5 from our gene-mapping analysis. To create the gene network (Fig. 5h), we use all default settings except that we use the recommended threshold for high-confidence interactions (0.700) for interaction scores. Singletons, i.e., genes not having any interactions with other ones, were not shown from the output network. We also used STRING to run functional enrichment analysis based on sources including Gene Ontology[96,97], Reactome Pathways[98] and KEGG[99].

eQTL tissue sharing analysis. We started with the rationale of our eQTL tissue sharing analysis. For simplicity, consider eQTLs found in one tissue (heart in our case), and we study the sharing of these eQTLs in a second tissue. Let p denote the probability of eQTLs in the first tissue being shared in the second tissue. Assuming we have several functional categories of eQTLs, e.g. regulatory elements specific in a cell type, or shared across cell types, we can then break down p into several categories with the simple relation:

$$p = \sum_c p_c w_c ,$$

where c denotes a category, p_c is the probability of tissue sharing in eQTLs from category c, and w_c is the proportion of eQTLs in category c. We hypothesize that different eQTLs categories have distinct molecular mechanisms of modulating transcript levels, and thus different tissue sharing patterns. This simple analysis thus suggests that both w_c and p_c are important for our understanding of tissue sharing. For instance, some categories may have a highly tissue-specific pattern (low p_c), but may constitute a small proportion of all eQTLs (low w_c), thus these categories would have limited contribution to the overall level of tissue sharing among eQTLs.

*Summary statistics of GTEx heart eQTLs***.** Summary statistics of eQTLs from the left ventricle were obtained from the GTEX v8 release[100]. We also obtained fine-mapping results using DAP-G[21]. The variants with posterior inclusion probability (PIP) greater than 0.8 were kept for downstream analyses. We refer to these putative causal variants as eQTLs henceforth. The total number of eQTL-gene pairs that passed the threshold is 1,216. Tissue sharing data on the same eQTLs were also obtained from GTEx[100]. These data provide information of whether these heart eQTLs are also associated with gene expression in the other tissues in GTEx.

Defining functional categories of heart eQTLs. eQTLs were intersected with genomic features. To obtain a set of disjoint genomic features, we used a combination of the union peak set and generic annotations. For generic annotations, the longest transcript was chosen for each gene body, and its corresponding exons, UTRs, and introns were obtained for all protein coding genes. We partitioned the union peak set into cell-type-specific categories based on the differential accessibility (DA) analysis, as well as the shared categories defined using the quantile approach, as described earlier. We note that DA analysis does not guarantee disjoint sets of features. Indeed, we find that cell types such as lymphoid and myeloid share about 6% of their DA peaks, while CMs share at most 1% with the other cell-types. To make these cell-type DA sets disjoint, we moved any DA peaks that occurred in multiple cell types from DA analysis, to the "Shared 2-3" and "Shared 4+" categories (see "Defining and classifying OCRs") depending on the number of cell types in which it occurred. A small percentage of peaks (< 1%) were affected by this step. The eQTLs in OCRs that overlap with exons or UTRs, or eQTLs in non-DA OCRs, are ambiguous to assign, so they were filtered from our analysis. The eQTLs in intronic OCRs were assigned based on the OCR

categories. Those eQTLs not intersecting with any functional category were designated in an "unassigned" category.

Estimating extent of tissue sharing in different categories of heart eQTLs. GTEx has performed eQTL mapping jointly across all tissues. Using these results, we call a SNP an eQTL in a given tissue, if it passes the local false sign rate (LFSR) threshold of 1%. For any eQTL, we can thus determine the number of tissues where it is active.

Estimating eQTL enrichment in functional categories. All the fine-mapped heart eQTLs are assigned to our set of categories. The proportion of eQTLs in each category is then compared with the expected proportion by chance to obtain enrichment reported in Fig. 6d and 6e. We used SNPsnap[101] to create a set of random control SNPs that match our eQTLs in LD and minor allele frequency. The LD data is obtained from the European population genotypes from 1000 Genomes. We generated 1000 random SNPs which is roughly how many high-confidence eQTLs were used. The proportion of random SNPs in each category is then used as our estimated proportion by chance.

Data availability

Our snRNA-seq and scATAC-seq data has been deposited in GEO repository: accession GSE224997.

Code availability

Mapgen R package is available from https://github.com/xinhe-lab/Mapgen. Code for data processing and analyses are available at https://github.com/xinhe-lab/heart_atlas.

Acknowledgements:

This work was funded by National Institutes of Health (NIH) grants, R01MH110531 and R01HG010773 (to X.H.), R01HL163523 (to X.H., S.P., and I.P.M.), and R21 AI144417-02 (to O.B). This project has been made possible in part by grant number CZF2019-002431 from the Chan Zuckerberg Initiative DAF, an advised fund of Silicon Valley Community Foundation. This work was completed in part with resources provided by the University of Chicago Research Computing Center. We thank Xuanyao Liu for helpful comments on the manuscript.

Main figures:

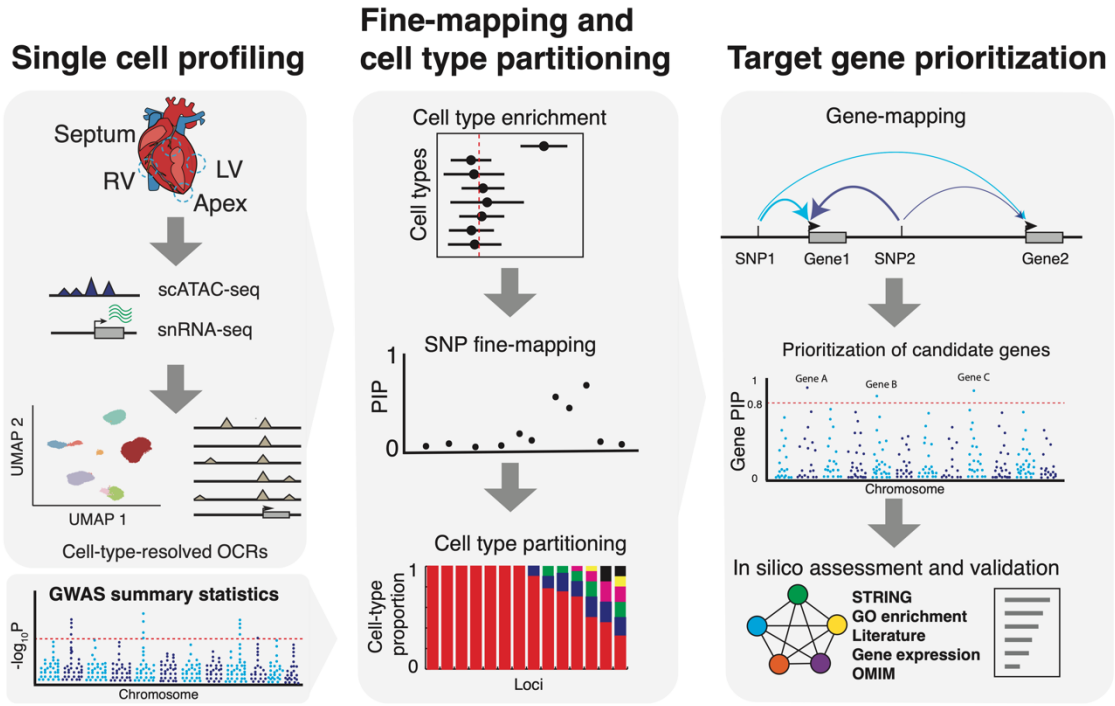

Fig. 1 | Overview of our experimental and computational framework. Left: SnRNA-seq and scATAC-seq profiling to cluster cells and obtain open chromatin regions (OCRs) in each cell type. **Middle:** Using OCRs and GWAS summary statistics to assess variant enrichment in cell-type-resolved OCRs. The enrichment results then provide prior for Bayesian statistical fine-mapping. The resulting Posterior Inclusion Probabilities (PIPs) represent the probabilities of variants being causal. The likely cell types through which the causal signals at each locus act can be identified by considering cell type information of likely causal variants. We may not always be able to identify a single cell type per locus, so we assign probabilities to cell types. **Right:** Computational gene-mapping using PIPs from SNP fine-mapping and SNP-to-gene links to obtain gene level PIPs. Note that the PIP of a SNP is partitioned into nearby genes in a weighted fashion, with more likely target genes receiving higher weights (as indicated by thicker arrows). Prioritized genes can be further assessed through external evidence such as gene networks and expression.

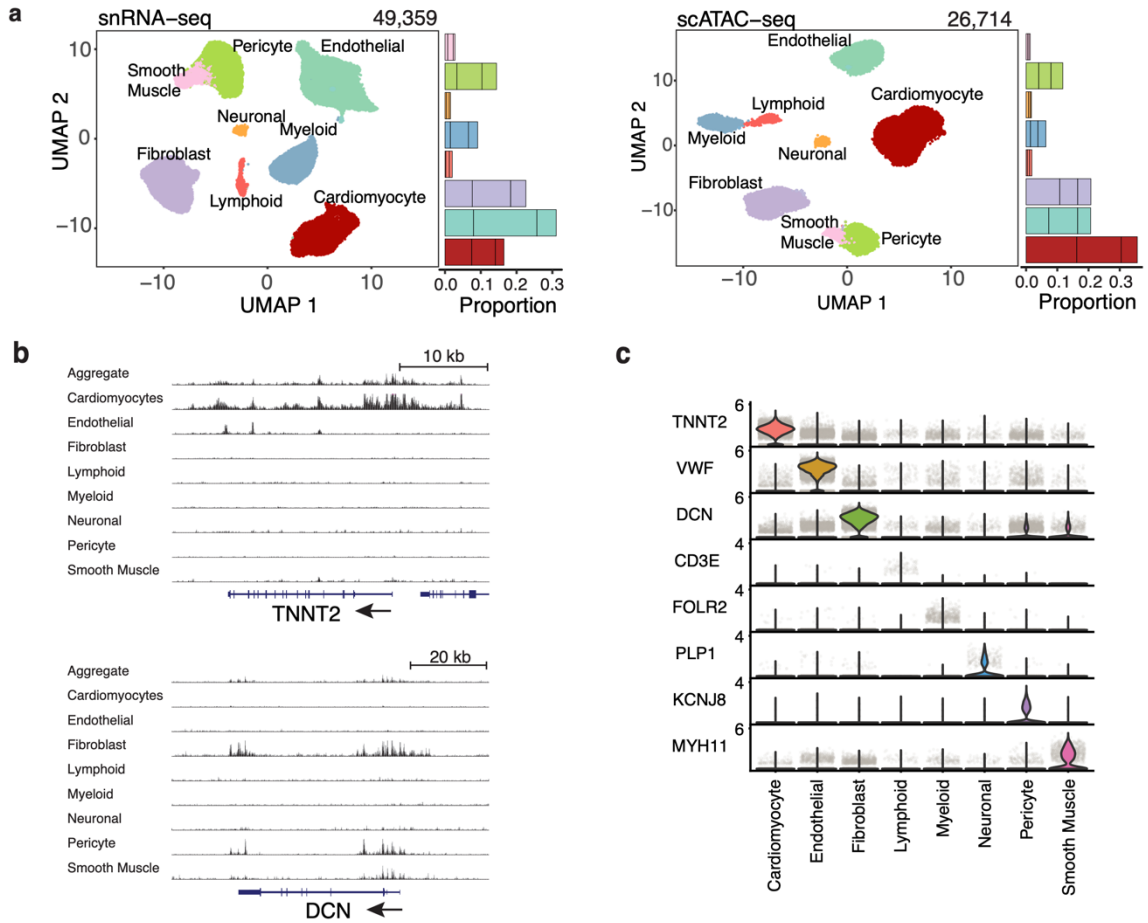

Fig. 2 | Mapping cell types in the human heart. a, UMAP projection of individual cells from snRNA-seq and scATAC-seq colored by cell types. Stacked barplots on the right represent the proportions of cell-types from each of the three donors. **b,** UCSC genome browser track plots of chromatin accessibility at selected marker genes across cell types. The bottom part shows the gene track (RefSeq annotation). Shown are two marker genes, TNNT2: cardiomyocyte marker; DCN: fibroblast marker. **c,** Stacked violin plots of marker gene expression (log-normalized expression values) in each cell type.

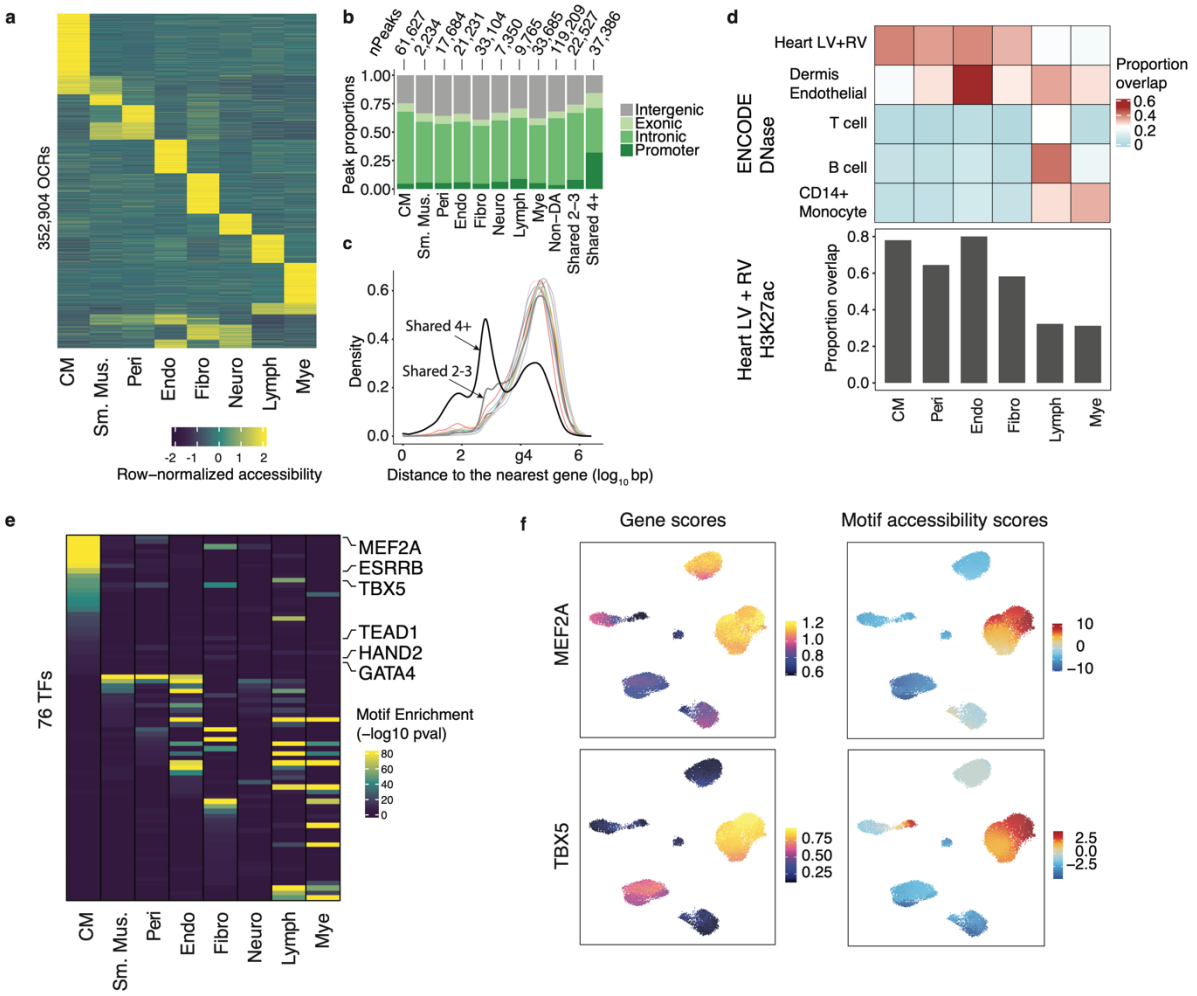

Fig. 3 | Discovery of OCRs and transcriptional regulators in the human heart. a, Row-normalized accessibility of OCRs across all cell types. **b,** Number of cell-type-specific and shared OCRs and their genomic distributions. **c,** Density plot of the $\log_{10}$ distance to nearest gene for all cell-type-specific and shared OCRs. Colors of the lines for cell-type-specific OCRs follow the same convention as in Figure 2a. Gray and black lines represent shared 2-3 and shared 4 OCRs. **d,** Proportions of cell-type specific OCRs that overlap with DHS (upper panel). Bar graph (lower panel) shows the proportions of cell-type specific OCRs that overlap with H3K27ac regions (LV = left ventricle, RV = right ventricle). Smooth muscle cells and neuronal cells are not shown due to the small numbers of peaks in these cell types. **e,** Enrichment of TF motifs in the OCRs specific to each cell type. Shown are 76 TFs with FDR < 1% from motif enrichment analysis in at least one cell-type, and correlation between motif enrichment and gene activity > 0.5. **f,** Gene scores (from ArchR) and motif accessibility scores calculated with chromVar in OCRs for MEF2A (top) and TBX5 (bottom) across all cells. Abbreviations for cell-types: CM = Cardiomyocyte, S.M = Smooth Muscle, Peri = Pericyte, Endo = Endothelial, Fibro = Fibroblast, Neuro = Neuronal, Mye = Myeloid, Lymph = Lymphoid.

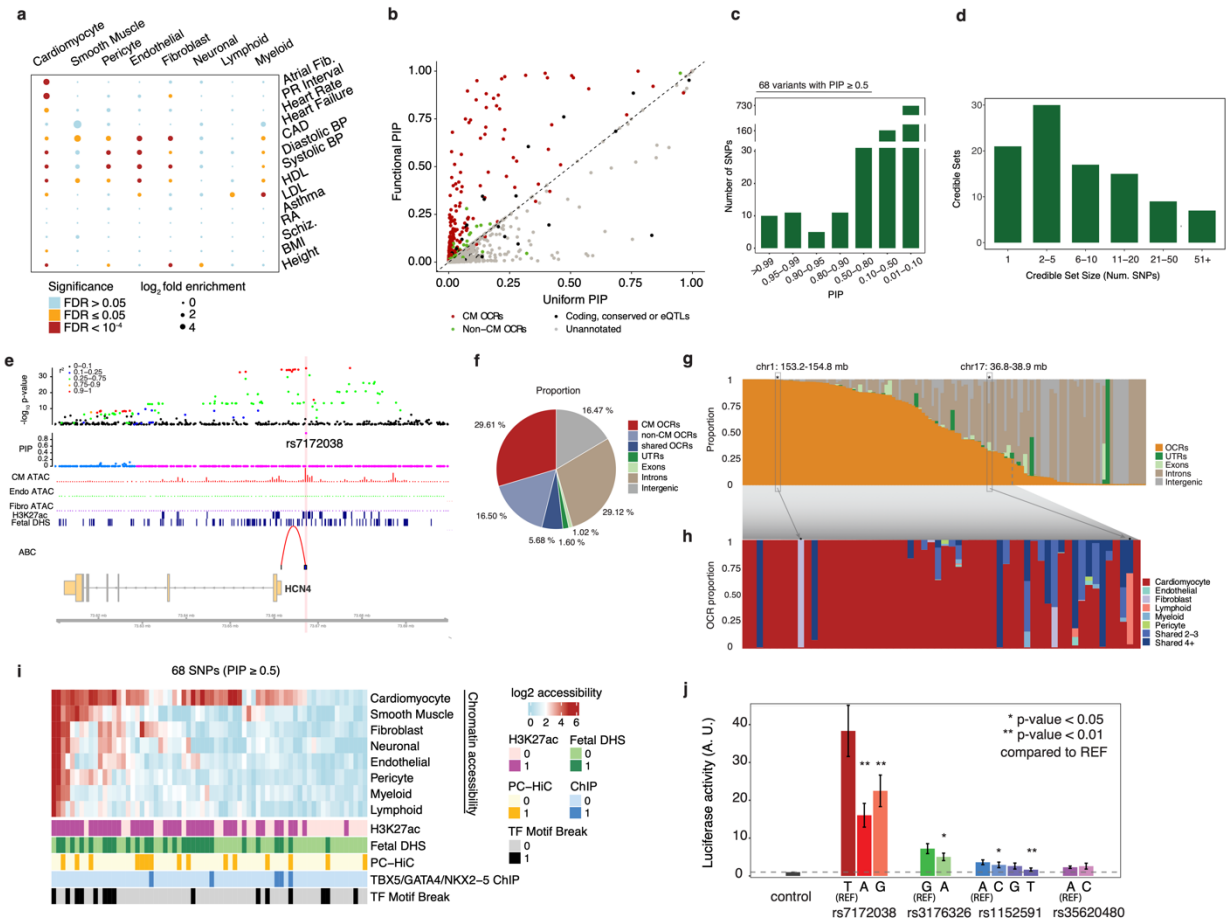

Fig. 4 | Statistical fine-mapping of loci associated with the AF risk. a, $\log_2$ fold enrichment (from the tool TORUS) of risk variants of various traits in cell-type-specific OCRs. **b,** Comparison of AF fine-mapping results under the informative prior using OCRs (Y-axis) vs. the results under the uniform prior (X-axis). Each dot is a SNP, and color represents the annotation of SNPs. Dashed line has a slope of 1. **c,** Summary of PIPs of variants. **d,** Summary of credible set sizes from fine-mapping of AF. **e,** Trackplot at the HCN4 locus and the finemapped variant rs7172038 (PIP = 0.99). The top two tracks represent the $-\log_{10}$ p-value of SNPs from AF GWAS (with color representing LD with the lead SNP) and their PIPs from SNP-level fine-mapping. Middle three tracks represent cell-type aggregated ATAC-seq signals (CM: red, endothelial: green; fibroblast: purple), followed by heart H3K27ac and fetal DHS peak calls. The bottom track represents ABC scores from the heart ventricle. Abbreviations for cell-types: CM = Cardiomyocyte, Endo = Endothelial, Fibro = Fibroblast. **f**, Proportions of summed PIPs in disjoint functional annotation categories among all the loci. **g**, Proportion of summed PIPs in disjoint functional annotation categories at each individual locus. **h**, Proportion of summed PIPs into cell type-specific OCRs at each individual locus, for loci with summed PIPs in OCR >= 0.25. Highlighted are two loci with high proportions in non-CM cells: fibroblast, lymphoid specific OCRs. **i,** Chromatin accessibility and additional functional genomic annotations of all SNPs with PIP >= 50%. **j**, Reporter activities in cardiac cells (HL-1) of regions containing selected SNPs, with both reference and alternative alleles. Data are from 5 replicates for each construct. P-values were calculated using a paired two-sided t-test.

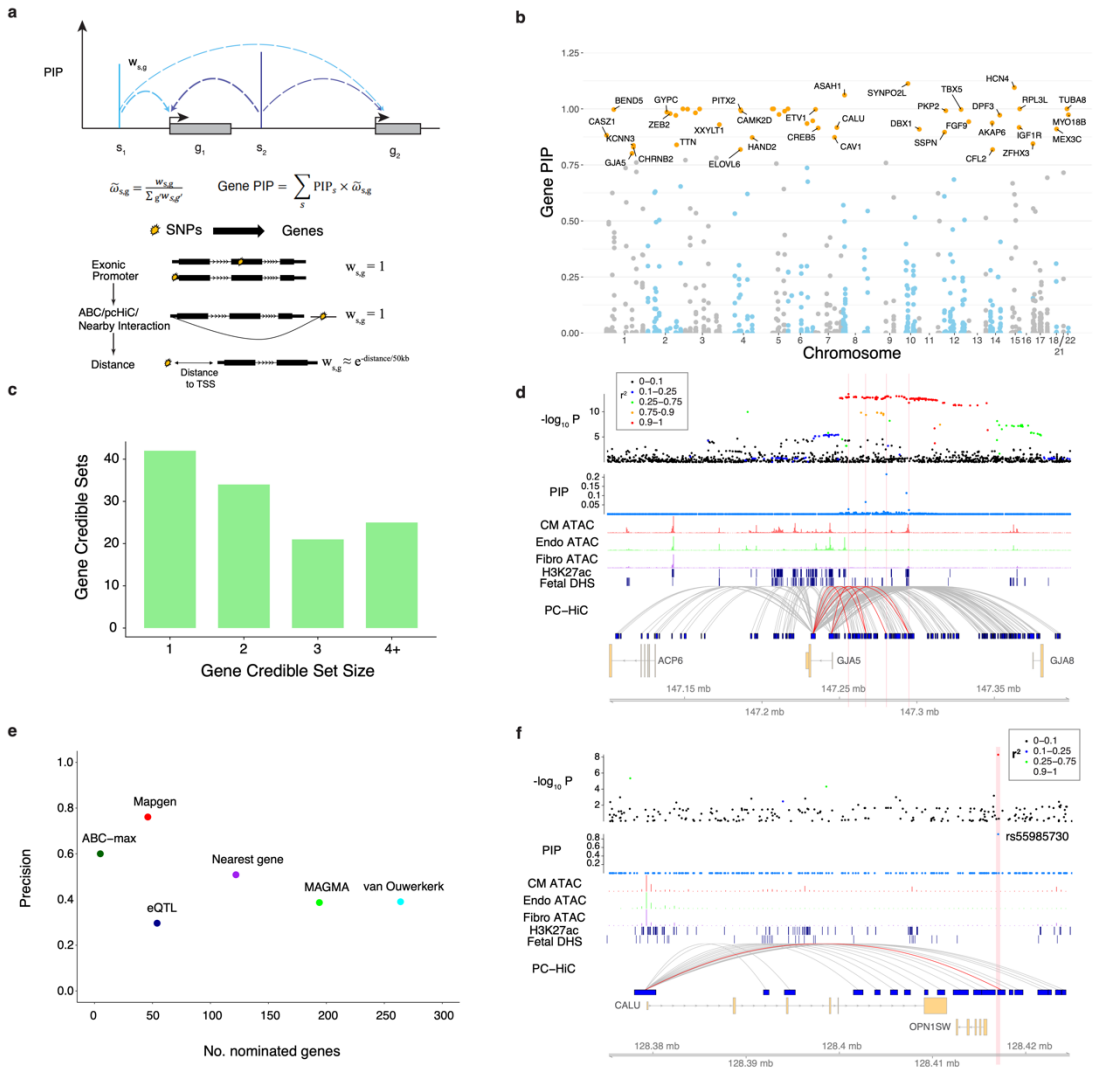

Fig. 5 | Mapping putative risk genes of AF. a. Schematic demonstrating the calculation of gene-level PIPs. g_1 and g_2 represent genes, and s_1, s_2 represent SNPs. Vertical bars show the PIPs of the SNPs from fine-mapping. Dashed arrows show the linking of SNPs to genes. $w_{s,g}$ represents the weight of a gene (g) with respect to a SNP (S). The PIP of a gene is the weighted sum of PIPs of SNPs that are linked to that gene. The weight of a SNP-gene pair is set according to the locations of the SNP relative to the gene. See Methods for details. **b,** Manhattan plot of gene PIPs. Genes at PIP >= 0.8 at labeled. **c,** Summary of the sizes of 80% credible gene sets from gene mapping. **d,** GJA5 locus: similar to Fig. 4e, except that the links here represent interactions identified from promoter-capture HiC data in iPSC-derived CMs. Vertical bars show the locations of the four fine-mapped SNPs supporting GJA5 as the risk gene in this locus. The red links in the PC-HiC track show interactions linked to these four fine-mapped SNPs. **e,** The performance of Mapgen and other methods in nominating AF risk genes. Precision is measured as the proportion of likely risk genes, those annotated with AF-related GO terms, in the set of nominated genes by each method. See Methods for the details of each method. **f,** CALU locus, tracks shown are similar to the panel **d.** The vertical bar shows the location of the top fine-mapped SNP. Abbreviations for cell-types: CM = Cardiomyocyte, Endo = Endothelial, Fibro = Fibroblast.

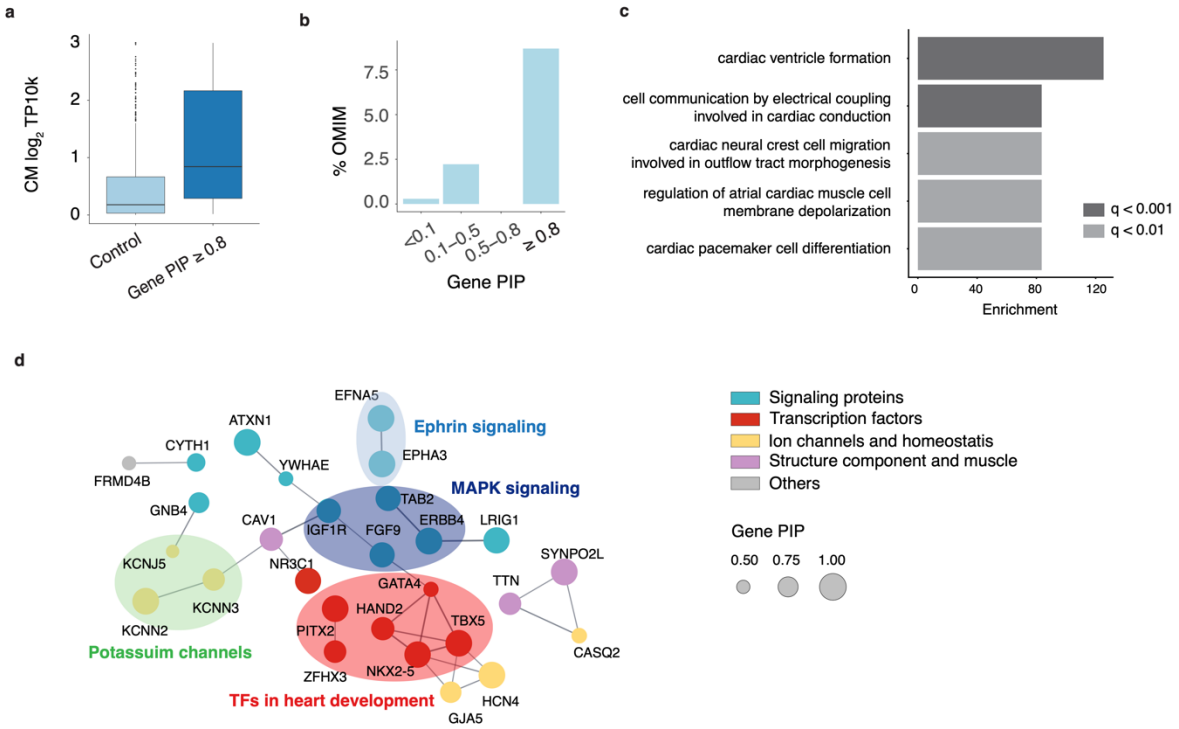

Fig. 6 | Functional support of putative AF risk genes. a, Log-normalized CM expression of genes at PIP >= 80% vs. other genes from the AF loci. **b,** Percentage of Mendelian disease genes from OMIM in each gene PIP bin. **c,** Top 5 Biological Processes (BP) and Molecular Functions (MF) GO terms from gene-set enrichment analysis of the 46 genes with PIP >= 80%. **d,** Gene interaction network of candidate AF genes (PIP >= 0.5) using STRING. Only genes with interactions are shown. Interactions are defined using a confidence threshold of 0.7 by STRING. Node sizes represent gene PIPs. Colors of genes indicate their shared molecular functions.

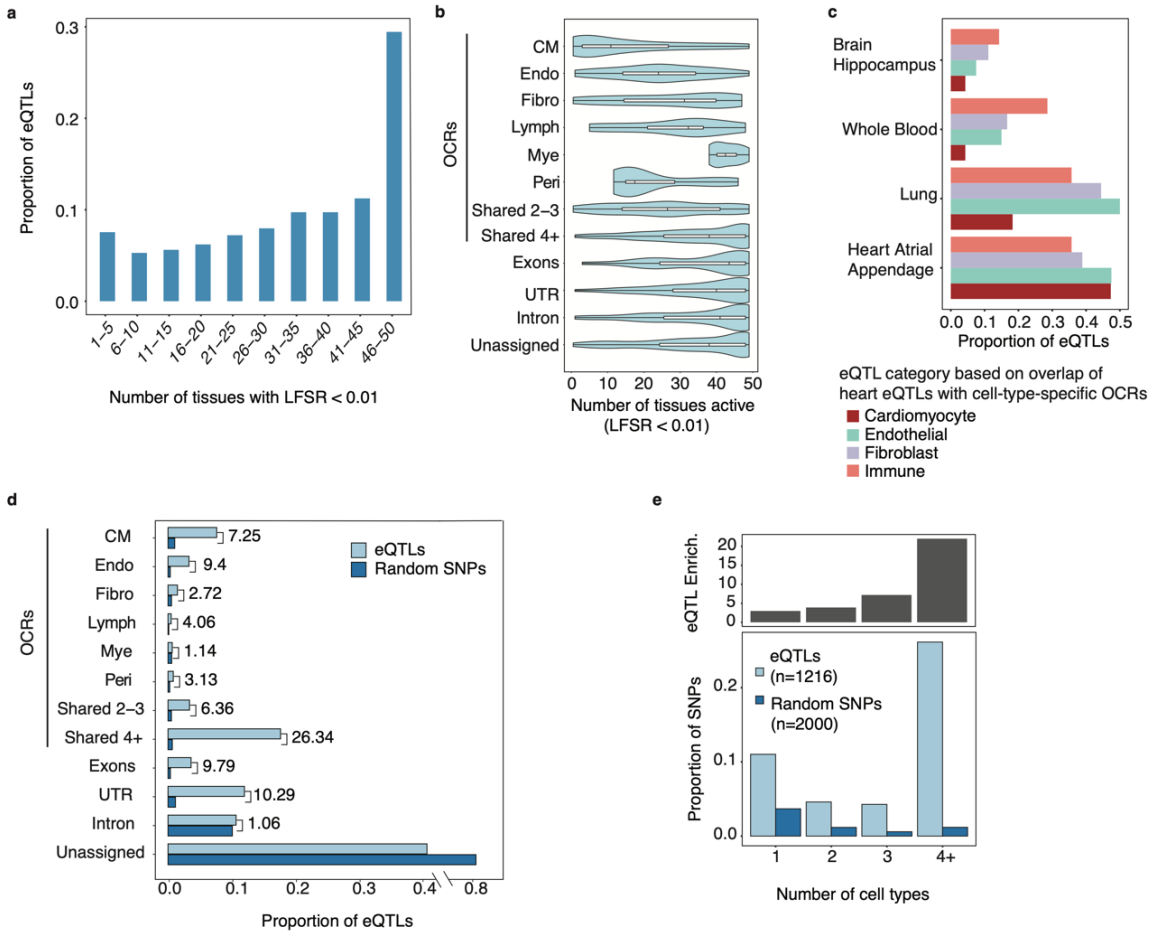

Fig. 7 | Tissue-sharing patterns of heart (LV) eQTLs from GTEx. a, Number of tissues where LV-eQTLs are detected at local false sign rate (LFSR) < 1%. **b,** Violin plot showing the number of tissues in which a specific eQTL is detected. Each row represents a different class of eQTLs, assigned based on their overlap with OCRs categories and other genomic locations. Unassigned: eQTLs that cannot be assigned to any functional class. **c,** Proportion of LV-eQTLs located in OCRs of selected cell types (Cardiomyocytes, Endothelial cells, Fibroblast, and Immune cells) that were also detected as eQTLs in a second tissue. **d,** Proportion of LV-eQTLs (n = 1216) in each functional class. For comparison, the proportions of random SNPs in all the classes are also shown. The numbers near the bars represent the fold enrichment in heart eQTLs compared to random SNPs. **e,** Enrichment of GTEx heart eQTLs in OCRs vary with the number of cell types where the OCRs are active. Lower panel shows the proportion of eQTLs (light blue) and control SNPs (dark blue, chosen to match eQTLs in LD and MAF) overlapping OCRs. The OCRs are divided into 4 categories, based on the degree of sharing across cell types in heart: 1= not shared, 4+= shared in >=4 cell types. The upper panel shows the enrichment of eQTLs in each OCR class compared to expectation based on control SNPs. Abbreviations for cell-types: CM = Cardiomyocyte, S.M = Smooth Muscle, Peri = Pericyte, Endo = Endothelial, Fibro = Fibroblast, Neuro = Neuronal, Mye = Myeloid, Lymph = Lymphoid.

1015
1016 **Table 1 | Top prioritized genes (gene PIP >= 0.95).**
1017
1018

Gene	Gene PIP	Supporting SNPs	SNP PIP	Link Method*	OMIM	CM-specific expression	Known AF risk gene	Reference
SYNPO2L	1.113	rs60632610	0.971	exon			✓	[20215401, 33768119]
HCN4	1.095	rs7172038	0.989	ABC	✓		✓	[29987112]
ASAH1	1.061	rs7508	1	exon		✓		[32015399]
ATXN1	1.000	rs59430691	0.809	PC-HiC				[21475249, 22306179]
ERBB4	1.000	rs6738011	0.12	distance		✓		[19632177]
KCNN2	1.000	rs337705 rs337708	0.528 0.113	distance distance			✓	[19139040]
RPL3L	1.000	rs140185678	1	exon				[32870709, 32514796]
TUBA8	1.000	rs464901 rs361834	0.886 0.114	nearby OCR nearby OCR				[31398994]
EPHA3	0.999	rs35124509 rs6771054 rs2117137	0.345 0.1720.117	exons distance distance				[17046737]
THRB	0.999	rs73041705 rs73032363 rs9841040 rs1865712	0.177 0.139 0.130 0.119	distance distance distance distance		✓		[28740583]
ETV1	0.998	rs55734480 rs12154315 rs12112152	0.403 0.338 0.218	distance distance distance			✓	[27775552, 29930145]
BEND5	0.997	rs11590635	0.973	distance				
PITX2	0.997	rs1906615 rs7689774	0.798 0.15	distance distance			✓	[28217939, 29367545, 32309338]
TBX5	0.997	rs7312625 rs883079 rs7955405	0.511 0.194 0.126	distance exon PC-HiC		✓	✓	[28057264]

PKP2	0.992	rs12809354 rs2045172	0.771 0.211	PC-HiC PC-HiC		✓		[28740174]
CAMK2D	0.991	rs11938486 rs17446418	0.649 0.17	distance PC-HiC		✓	✓	[24030498]
NKX2-5	0.989	rs6882776 rs6891790 rs2277923 rs10071514	0.37 0.318 0.157 0.133	active promoter ABC/nearby OCR exon ABC/nearby OCR	✓			[26805889]
GYPC	0.985	rs28387148 rs28387129 rs28387153 rs28387149	0.191 0.153 0.144 0.103	distance nearby OCR distance distance				
LRIG1	0.982	rs34080181 rs900171 rs12633819	0.329 0.119 0.106	distance exon distance				[23558895, 19632177]
ZEB2	0.979	rs10496971	0.896	distance				[33398012]
NR3C1	0.975	rs72804738	0.208	distance				[23595884]
MYO18B	0.974	rs133902 rs133885	0.685 0.185	distance exon		✓		[27858739]
DPF3	0.972	rs3814866 rs3814864	0.744 0.176	active promoter active promoter		✓	✓	[26582913, 30240284]
WIPF1	0.971	rs35215597	0.874	Nearby OCR				

* In the Supporting SNPs column, only SNPs that contribute a fractional PIP (SNP PIP multiplied by the weight of the SNP to that gene) of 0.1 or more are shown. *EFNA5* (gene PIP =1) is not included because it does not have any SNPs with fractional PIP >= 0.1.
* Nearby OCR is defined as OCR within 20 kb of active promoter of the gene.
* Reference column shows the PMIDs of the relevant papers supporting the connections of the genes to AF or heart physiology.

References

1. Benjamin, E. J. *et al.* Independent Risk Factors for Atrial Fibrillation in a Population-Based

1031 Cohort: The Framingham Heart Study. *JAMA* **271**, 840–844 (1994).
1032 2. Kornej, J., Börschel, C. S., Benjamin, E. J. & Schnabel, R. B. Epidemiology of Atrial
1033 Fibrillation in the 21st Century. *Circ. Res.* **127**, 4–20 (2020).
1034 3. Roselli, C. et al. Multi-ethnic genome-wide association study for atrial fibrillation. *Nat. Genet.*
1035 **50**, 12**25**–**123**3 (2018).
1036 4. Roselli, C., Rienstra, M. & Ellinor, P. T. Genetics of Atrial Fibrillation in 2020. Circ. Res.
1037 127, 21–33 (2020).
1038 5. Nielsen, J. B. et al. Biobank-driven genomic discovery yields new insight into atrial
1039 fibrillation biology. Nat. Genet. 50, 1234–1239 (2018).
1040 6. Arking, D. E. et al. Genetic association study of QT interval highlights role for calcium
1041 signaling pathways in myocardial repolarization. Nat. Genet. **46**, 826–836 (2014).
1042 7. Pfeufer, A. et al. Genome-wide association study of PR interval. Nat. Genet. **42**, 1**53**–159
1043 (2010).
1044 8. Maurano, M. T. et al. Systematic Localization of Common Disease-Associated Variation in
1045 Regulatory DNA. *Science* **337**, 1190–1195 (2012).
1046 9. Pickrell, J. K. Joint Analysis of Functional Genomic Data and Genome-wide Association
1047 Studies of 18 Human Traits. *Am. J. Hum. Genet.* **94**, 559–573 (2014).
1048 10. Finucane, H. K. et al. Partitioning heritability by functional annotation using genome-wide
1049 association summary statistics. Nat. Genet. **47**, 1228–1235 (2015).
1050 11. Kundaje, A. et al. Integrative analysis of 111 reference human epigenomes. *Nature* **518**, 317–
1051 330 (2015).
1052 12. Consortium, E. P. et al. Expanded encyclopaedias of DNA elements in the human and mouse
1053 genomes. Nature **583**, 699–710 (2020).
1054 13. Ouwerkerk, A. F. van et al. Identification of atrial fibrillation associated genes and functional
1055 non-coding variants. *Nat. Commun.* **10**, 4755 (201**9**).
1056 14. Ouwerkerk, A. F. van et al. Identification of Functional Variant Enhancers Associated With
1057 Atrial Fibrillation. Circ. Res. 127, 229–243 (2020).
1058 15. Hocker, J. D. et al. Cardiac cell type–specific gene regulatory programs and disease risk
1059 association. *Sci. Adv.* **7**, eabf1444 (2021).
1060 16. Habib, N. et al. Massively-parallel single nucleus RNA-seq with DroNc-seq. *Nat. Methods*
1061 **14**, 955–958 (2017).
1062 17. Litviňuková, M. et al. *Cell*s of the adult human heart. Nature **588**, 466–472 (2020).
1063 18. Tucker, N. R. et al. Transcriptional and Cellular Diversity of the Human Heart. *Circulation*
1064 **142**, 466–482 (2020).
1065 19. Buenrostro, J. D. et al. Single-cell chromatin accessibility reveals principles of regulatory
1066 variation. Nature **523**, 486–490 (2015).
1067 20. Cusanovich, D. A. et al. Multiplex single cell profiling of chromatin accessibility by
1068 combinatorial cellular indexing. Science **348**, 910–914 (2015).
1069 21. Wen, X., Lee, Y., Luca, F. & Pique-Regi, R. Efficient Integrative Multi-SNP Association
1070 Analysis via Deterministic Approximation of Posteriors. Am. J. Hum. Genet. **98**, 1114–1129

1071 (2016).
1072 22. Weissbrod, O. et al. Functionally informed fine-mapping and polygenic localization of
1073 complex trait heritability. Nat. Genet. 52, 1355–1363 (2020).
1074 23. Mahajan, A. et al. Fine-mapping type 2 diabetes loci to single-variant resolution using high-
1075 density imputation and islet-specific epigenome maps. Nat. Genet. 50, 1505–1513 (2018).
1076 24. Trubetskoy, V. et al. Mapping genomic loci implicates genes and synaptic biology in
1077 schizophrenia. Nature **604**, 502–508 (2022).
1078 25. Huang, H. et al. Fine-mapping inflammatory bowel disease loci to single-variant resolution.
1079 Nature **547**, **173**–178 (2017).
1080 26. Segrè, A. V. et al. Common Inherited Variation in Mitochondrial Genes Is Not Enriched for
1081 Associations with Type 2 Diabetes or Related Glycemic Traits. *Plos Genet* **6**, e1001058 (2010).
1082 27. Leeuw, C. A. de, Mooij, J. M., Heskes, T. & Posthuma, D. MAGMA: Generalized Gene-Set
1083 Analysis of GWAS Data. *Plos Comput Biol* **11**, e1004219 (2015).
1084 28. Butler, A., Hoffman, P., Smibert, P., Papalexi, E. & Satija, R. Integrating single-cell
1085 transcriptomic data across different conditions, technologies, and species. *Nat. Biotechnol.* **36**,
1086 411–420 (2018).
1087 29. Granja, J. M. et al. ArchR is a scalable software package for integrative single-cell chromatin
1088 accessibility analysis. Nat. Genet. 53, 403–411 (2021).
1089 30. Thurman, R. E. et al. The accessible chromatin landscape of the human genome. Nature **489**,
1090 75–82 (2012).
1091 31. Buenrostro, J. D. et al. Integrated Single-Cell Analysis Maps the Continuous Regulatory
1092 Landscape of Human Hematopoietic Differentiation. Cell 173, 1535-1548.e16 (2018).
1093 32. Schep, A. N., Wu, B., Buenrostro, J. D. & Greenleaf, W. J. chromVAR: inferring
1094 transcription-factor-associated accessibility from single-cell epigenomic data. *Nat Methods* **14**,
1095 975–978 (2017).
1096 33. Olson, E. N. Gene regulatory networks in the evolution and development of the heart.
1097 Science **313**, 1922–7 (2006).
1098 34. Wen, X. Molecular QTL discovery incorporating genomic annotations using Bayesian false
1099 discovery rate control. *Ann. Appl. Statistics* **10**, **16**19–1638 (2016).
1100 35. Cheng, S. et al. Long-term Outcomes in Individuals With Prolonged PR Interval or First-
1101 Degree Atrioventricular Block. JAMA **301**, 2571–2**577** (2009).
1102 36. Yu, F. et al. Variant to function mapping at single-cell resolution through network
1103 propagation. *Nat Biotechnol* 1–10 (2022) doi:10.1038/s4**158**7-022-01341-y.
1104 **37**. Berisa, T. & Pickrell, J. K. Approximately independent linkage disequilibrium blocks in
1105 human populations. *Bioinformatics* **32**, 283–285 (2016).
1106 38. Wang, G., Sarkar, A., Carbonetto, P. & Stephens, M. A simple new approach to variable
1107 selection in regression, with application to genetic fine mapping. *J. R. Stat. Soc. Ser. B.*
1108 *Statistical Methodol.* **82**, 1273–1300 (2020).
1109 39. Nasser, J. et al. Genome-wide enhancer maps link risk variants to disease genes. Nature **593**,
1110 238–243 (2021).

1111 40. Ouwerkerk, A. F. van et al. Epigenetic and Transcriptional Networks Underlying Atrial
1112 Fibrillation. Circ. Res. 127, 34–50 (2020).
1113 41. Sobreira, D. R. et al. Extensive pleiotropism and allelic heterogeneity mediate metabolic
1114 effects of IRX3 and IRX5. Science **372**, 1085–1091 (2021).
1115 42. Montefiori, L. E. et al. A promoter interaction map for cardiovascular disease genetics. *Elife*
1116 **7**, e35788 (2018).
1117 43. Kapoor, A. et al. Multiple SCN5A variant enhancers modulate its cardiac gene expression
1118 and the QT interval. *Proc. Natl. Acad. Sci. U.S.A.* **116**, 201808734 (2019).
1119 44. Claycomb, W. C. et al. HL-1 cells: A cardiac muscle cell line that contracts and retains
1120 phenotypic characteristics of the adult cardiomyocyte. Proc. Natl. Acad. Sci. U.S.A. **95**, 2979–
1121 2984 (1998).
1122 45. DiFrancesco, D. HCN4, Sinus Bradycardia and Atrial Fibrillation. *Arrhythmia Electrophysiol*
1123 *Rev.* **4**, 9 (2015).
1124 46. Giambartolomei, C. et al. Bayesian Test for Colocalisation between Pairs of Genetic
1125 Association Studies Using Summary Statistics. *PLoS Genet.* **10**, e1004383 (2014).
1126 47. Claussnitzer, M. et al. A brief history of human disease genetics. Nature 577, 179–189
1127 (2020).
1128 48. Nadadur, R. D. et al. Pitx2 modulates a Tbx5 -dependent gene regulatory network to
1129 maintain atrial rhythm. *Sci Transl Med* **8**, 354ra115 (2016).
1130 49. Drabkin, M. et al. Nocturnal Atrial Fibrillation Caused by Mutation in KCND2 , Encoding
1131 Pore-Forming (α) Subunit of the Cardiac Kv4.2 Potassium Channel. *Circulation Genom Precis*
1132 *Medicine* **11**, e002293 (2018).
1133 50. Mahida, S. et al. Overexpression of KCNN3 results in sudden cardiac death. *Cardiovasc Res*
1134 **101**, 326–334 (2013).
1135 51. H., G. M. et al. Somatic Mutations in the Connexin 40 Gene (GJA5) in Atrial Fibrillation.
1136 *New Engl J Med* **354**, 2677–2688 (2006).
1137 52. Chung, I.-M. & Rajakumar, G. Genetics of Congenital Heart Defects: The NKX2-5 Gene, a
1138 Key Player. *Genes (Basel).* **7**, 6 (2016).
1139 53. Sahoo, S. K. & Kim, D. H. Characterization of calumenin in mouse heart. *BMB Rep.* **43**,
1140 158–63 (2010).
1141 54. Lee, J. H., Kwon, E. J. & Kim, D. H. Calumenin has a role in the alleviation of ER stress in
1142 neonatal rat cardiomyocytes. *Biochem Bioph Res Co* **439**, 327–332 (2013).
1143 55. Sirish, P., Diloretto, D. A., Thai, P. N. & Chiamvimonvat, N. The Critical Roles of
1144 Proteostasis and Endoplasmic Reticulum Stress in Atrial Fibrillation. *Front Physiol* **12**, 79**31**71
1145 (2022).
1146 56. Ahlberg, G. et al. Rare truncating variants in the sarcomeric protein titin associate with
1147 familial and early-onset atrial fibrillation. Nat. Commun. 9, **4**316 (2018).
1148 57. Choi, S. H. et al. Monogenic and Polygenic Contributions to Atrial Fibrillation Risk. *Circ*
1149 *Res* **126**, 200–209 (2020).
1150 58. Szklarczyk, D. et al. STRING v11: protein–protein association networks with increased

1151 coverage, supporting functional discovery in genome-wide experimental datasets. *Nucleic Acids*
1152 *Res.* **47**, gky1131 (2018).
1153 59. Benaglio, P. et al. Allele-specific NKX2-5 binding underlies multiple genetic associations
1154 with human electrocardiographic traits. Nat. Genet. 51, 1506–1517 (2019).
1155 60. Schindler, Y. L. et al. Hand2 elevates cardiomyocyte production during zebrafish heart
1156 development and regeneration. *Development* **141**, 3112–3122 (2014).
1157 61. Cohen, A. S. A. et al. Haploinsufficiency of the basic helix–loop–helix transcription factor
1158 HAND2 causes congenital heart defects. *Am. J. Med. Genet.* **182**, 1263–1267 (2020).
1159 62. Romero-Becerra, R., Santamans, A. M., Folgueira, C. & Sabio, G. p38 MAPK Pathway in
1160 the Heart: New Insights in Health and Disease. *Int. J. Mol. Sci.* **21**, 7412 (2020).
1161 63. O'Neal, W. T. et al. Ephrin–Eph signaling as a potential therapeutic target for the treatment
1162 of myocardial infarction. *Med. Hypotheses* **80**, 738–744 (2013).
1163 64. Su, S. et al. Essential roles of EphrinB2 in mammalian heart: from development to diseases.
1164 *Cell Commun. Signal.* **17**, 29 (2019).
1165 65. Chen, K. et al. EphB4 Forward-Signaling Regulates Cardiac Progenitor Development in
1166 Mouse ES Cells. *J Cell Biochem* **116**, 467–475 (2015).
1167 66. Chun, S. et al. Limited statistical evidence for shared genetic effects of eQTLs and
1168 autoimmune disease-associated loci in three major immune cell types. *Nat Genet* **49**, 600–605
1169 (2017).
1170 67. Yao, D. W., O'Connor, L. J., Price, A. L. & Gusev, A. Quantifying genetic effects on disease
1171 mediated by assayed gene expression levels. Nat. Genet. 52, 626–633 (2020).
1172 68. Umans, B. D., Battle, A. & Gilad, Y. Where Are the Disease-Associated eQTLs? *Trends*
1173 *Genet* **37**, 109–124 (2021).
1174 69. Chiou, J. et al. Single-cell chromatin accessibility identifies pancreatic islet cell type– and
1175 state-specific regulatory programs of diabetes risk. Nat Genet **53**, **45**5–466 (2021).
1176 70. Lozano-Velasco, E., Franco, D., Aranega, A. & Daimi, H. Genetics and Epigenetics of Atrial
1177 Fibrillation. *Int J Mol Sci* **21**, 5717 (2020).
1178 71. Wang, J., Gareri, C. & Rockman, H. A. G-Protein–Coupled Receptors in Heart Disease. Circ.
1179 Res. 123, 716–735 (2018).
1180 72. Foulquier, S. et al. WNT Signaling in Cardiac and Vascular Disease. *Pharmacol Rev* **70**, 68–
1181 141 (2018).
1182 73. Huang, J. et al. Fibroblast growth factor 9 (FGF9) inhibits myogenic differentiation of
1183 C2C12 and human muscle cells. *Cell Cycle* **18**, 1–19 (2019).
1184 74. Itoh, N. & Ohta, H. Pathophysiological roles of FGF signaling in the heart. Front Physiol 4,
1185 247 (2013).
1186 75. Nattel, S. Molecular and Cellular Mechanisms of Atrial Fibrosis in Atrial Fibrillation. *JACC*
1187 *Clin. Electrophysiol.* **3**, 425–435 (2017).
1188 76. Chromium Single Cell 3' Reagent Kits User Guide (v3.1 Chemistry).
1189 https://support.10xgenomics.com/single-cell-gene-expression/library-prep/doc/user-guide-
1190 chromium-single-cell-3-reagent-kits-user-guide-v31-chemistry (2019).

1191 77. Selewa, A. et al. Systematic Comparison of High-throughput Single-Cell and Single-Nucleus
1192 Transcriptomes during Cardiomyocyte Differentiation. *Sci. Rep.* **10**, 1535 (2020).
1193 78. FastQC. https://qubeshub.org/resources/fastqc (2015).
1194 79. Andrews, S. FastQC: A Quality Control Tool for High Throughput Sequence Data [Online].
1195 http://www.bioinformatics.babraham.ac.uk/projects/fastqc/ (2010).
1196 80. Kaminow, B., Yunusov, D. & Dobin, A. STARsolo: accurate, fast and versatile
1197 mapping/quantification of single-cell and single-nucleus RNA-seq data. *Biorxiv*
1198 2021.05.05.442755 (2021) doi:10.1101/2021.05.05.442755.
1199 81. Frankish, A. et al. GENCODE reference annotation for the human and mouse genomes.
1200 Nucleic Acids Res 47, gky955- (2018).
1201 82. Stuart, T. et al. Comprehensive Integration of Single-Cell Data. Cell **177**, 1888-1902.e21
1202 (2019).
1203 83. McGinnis, C. S., Murrow, L. M. & Gartner, Z. J. DoubletFinder: Doublet Detection in
1204 Single-Cell RNA Sequencing Data Using Artificial Nearest Neighbors. *Cell Syst* **8**, 329-337.e4
1205 (2019).
1206 84. Satpathy, A. T. et al. Massively parallel single-cell chromatin landscapes of human immune
1207 cell development and intratumoral T cell exhaustion. Nat. Biotechnol. 37, 925–936 (2019).
1208 85. Korsunsky, I. et al. Fast, sensitive and accurate integration of single-cell data with Harmony.
1209 Nat Methods 16, 1**28**9–1296 (2019).
1210 86. Zhang, Y. et al. Model-based Analysis of ChIP-Seq (MACS). *Genome Biol.* **9**, R137–R137
1211 (2008).
1212 87. Lawrence, M. et al. Software for computing and annotating genomic ranges. *PLoS Comput.*
1213 *Biol.* **9**, e1003118 (2013).
1214 88. Weirauch, M. T. et al. Determination and Inference of Eukaryotic Transcription Factor
1215 Sequence Specificity. Cell 158, 1431–1443 (2014).
1216 89. Pliner, H. A. et al. Cicero Predicts cis-Regulatory DNA Interactions from Single-Cell
1217 Chromatin Accessibility Data. *Mol. Cell.* **71**, 858-871.e8 (2018).
1218 90. Lindblad-Toh, K. et al. A high-resolution map of human evolutionary constraint using 29
1219 mammals. Nature **478**, 476–82 (2011).
1220 91. Clarke, L. et al. The international Genome sample resource (IGSR): A worldwide collection
1221 of genome variation incorporating the 1000 Genomes Project data. Nucleic Acids Res 45, D854–
1222 D859 (2017).
1223 92. Coetzee, S. G., Coetzee, G. A. & Hazelett, D. J. motifbreakR: an R/Bioconductor package for
1224 predicting variant effects at transcription factor binding sites. Bioinformatics 31, 3847–3849
1225 (2015).
1226 93. Fulco, C. P. et al. Activity-by-contact model of enhancer–promoter regulation from
1227 thousands of CRISPR perturbations. Nat Genet **51**, 1664–1669 (2019).
1228 94. Szklarczyk, D. et al. The STRING database in 2021: customizable protein–protein networks,
1229 and functional characterization of user-uploaded gene/measurement sets. Nucleic Acids Res. 49,
1230 gkaa1074- (2020).

1231 95. Shannon, P. et al. Cytoscape: A Software Environment for Integrated Models of
1232 Biomolecular Interaction Networks. *Genome Res.* **13**, 2498–2504 (2003).
1233 96. Ashburner, M. et al. Gene Ontology: tool for the unification of biology. Nat. Genet. 25, 25–
1234 29 (2000).
1235 97. Consortium, T. G. O. et al. The Gene Ontology resource: enriching a GOld mine. Nucleic
1236 Acids Res 49, D325–D334 (2020).
1237 98. Jassal, B. et al. The reactome pathway knowledgebase. Nucleic Acids Res **48**, D498–D503
1238 (2019).
1239 99. Kanehisa, M. & Goto, S. KEGG: Kyoto Encyclopedia of Genes and Genomes. Nucleic Acids
1240 Res 28, 27–30 (2000).
1241 100. Consortium, T. Gte. The GTEx Consortium atlas of genetic regulatory effects across human
1242 tissues. Science **369**, 1318–1330 (2020).
1243 101. Pers, T. H., Timshel, P. & Hirschhorn, J. N. SNPsnap: a Web-based tool for identification
1244 and annotation of matched SNPs. Bioinformatics 31, 418–420 (2015).